ELSEVIER

Palaeogeography, Palaeoclimatology, Palaeoecology 182 (2002) 259–286

PALAEO

www.elsevier.com/locate/palaeo

Radiolarian-based paleotemperatures during the last 160 kyr at ODP Site 1089 (Southern Ocean, Atlantic Sector)

G. Cortese *, A. Abelmann

Alfred Wegener Institute for Polar and Marine Research (AWI), Columbusstrasse, P.O. Box 120161, 27515 Bremerhaven, Germany

Received 3 August 2000; accepted 5 December 2001

Abstract

Two cores, Site 1089 (ODP Leg 177) and PS2821-1, recovered from the same location (40°56′S; 9°54′E) at the Subtropical Front (STF) in the Atlantic Sector of the Southern Ocean, provide a high-resolution climatic record, with an average temporal resolution of less than 600 yr. A multi-proxy approach was used to produce an age model for Core PS2821-1, and to correlate the two cores. Both cores document the last climatic cycle, from Marine Isotopic Stage 6 (MIS 6, ca. 160 kyr BP, ka) to present. Summer sea-surface temperatures (SSSTs) have been estimated, with a standard error of ca. ±1.16°C, for the down core record by using Q-mode factor analysis (Imbrie and Kipp method). The paleotemperatures show a 7°C warming at Termination II (last interglacial, transition from MIS 6 to MIS 5). This transition from glacial to interglacial paleotemperatures (with maximum temperatures ca. 3°C warmer than present at the core location) occurs earlier than the corresponding shift in $\delta^{18}O$ values for benthic foraminifera from the same core; this suggests a lead of Southern Ocean paleotemperature changes compared to the global ice-volume changes, as indicated by the benthic isotopic record. The climatic evolution of the record continues with a progressive temperature deterioration towards MIS 2. High-frequency, millennial-scale climatic instability has been documented for MIS 3 and part of MIS 4, with sudden temperature variations of almost the same magnitude as those observed at the transitions between glacial and interglacial times. These changes occur during the same time interval as the Dansgaard–Oeschger cycles recognized in the $\delta^{18}O_{ice}$ record of the GRIP and GISP ice cores from Greenland, and seem to be connected to rapid changes in the STF position in relation to the core location. Sudden cooling episodes ('Younger Dryas (YD)-type' and 'Antarctic Cold Reversal (ACR)-type' of events) have been recognized for both Termination I (ACR-I and YD-I events) and II (ACR-II and YD-II events), and imply that our core is located in an optimal position in order to record events triggered by phenomena occurring in both hemispheres. Spectral analysis of our SSST record displays strong analogies, particularly for high, sub-orbital frequencies, to equivalent records from Vostok (Antarctica) and from the Subtropical North Atlantic ocean. This implies that the climatic variability of widely separated areas (the Antarctic continent, the Subtropical North Atlantic, and the Subantarctic South Atlantic) can be strongly coupled and co-varying at millennial time scales (a few to 10-ka periods), and eventually induced by the same triggering mechanisms. Climatic variability has also been documented for supposedly warm and stable interglacial intervals (MIS 1 and 5), with several cold events which can be correlated to other Southern Ocean and North Atlantic sediment records.

Keywords: radiolaria; paleotemperature; Southern Ocean; Antarctic Cold Reversal; Younger Dryas; Dansgaard–Oeschger cycles

* Corresponding author. Tel.: +49-471-4831-1207. *E-mail address:* gcortese@awi-bremerhaven.de (G. Cortese).

0031-0182/02/$ – see front matter
PII: S0031-0182(01)00499-0

1. Introduction

The sediments recovered from ODP Site 1089 and PS2821-1, at the South Atlantic Subtropical Front (STF), have an average sedimentation rate of 0.15 m/kyr for the last 160 ka. This high-resolution record provides the opportunity to focus on:

– the existence of rapid climate oscillations in the surface water of the Southern Hemisphere;

– the detailed structure of the last two glacial/interglacial transitions; and

– the climatic variability during the last two climatic optima (Marine Isotopic Stages (MIS) 1 and 5e).

Rapid climate change (Dansgaard–Oeschger (D–O) cycles) has been documented in Greenland ice cores (Johnsen et al., 1992; Chappellaz et al., 1993; Dansgaard et al., 1993) as well as in marine core records of the North Atlantic (Bond et al., 1993; McManus et al., 1994; Cortijo et al., 1995; Adkins et al., 1997; Fronval and Jansen, 1997; Lototskaya and Ganssen, 1999). Alterations of the North Atlantic thermohaline circulation are thought to be responsible for these rapid climatic changes, and the synchronism between the North Atlantic and the Greenland ice-sheet records seems to support, at least partly, this hypothesis. Recent ocean–atmosphere coupled models show that North Atlantic Deep Water (NADW) changes have an impact on Southern Hemisphere summer sea-surface temperatures (SSST), since the cross-equatorial heat transport is related to the thermohaline circulation strength (Crowley, 1992; Schiller et al., 1997). Rapid climatic oscillations have also been documented in the marine benthic and planktic $\delta^{18}O$ and $\delta^{13}C$ records of South Atlantic deep-sea cores (Charles et al., 1996; Ninnemann et al., 1999; Mortyn et al., submitted). These data suggest that millennial-scale NADW variability is reflected in the Southern Ocean deep-water signal, partly confirming the antiphase relationship between both hemispheres predicted by the models, but lagged the $\delta^{18}O$ surface-water signal by about 1500 yr. Southern Ocean sediment records do not therefore validate a direct link between short-term climatic variability in high latitudes of both hemispheres, since (a) the Northern Hemisphere climate signal lags that of the Southern Hemisphere by 1500 yr, and (b) in the Southern Hemisphere, poleward excursions of warmer surface waters do not always occur during periods of reduced NADW production (Ninnemann et al., 1999). The variability shown in the Southern Ocean planktic $\delta^{18}O$ signal (Charles et al., 1996; Ninnemann et al., 1999; Mortyn et al., submitted), possibly also influenced by changes in the surface current pattern and in the wind system, has not yet been documented in the paleotemperature record. This would represent an independent estimate of past surface hydrographic conditions, as it is not directly affected by either the global ice-volume signal or local salinity changes.

Another interesting issue in climatic research is the different warming trend from full glacial to interglacial conditions (terminations) between both the ice-core records from the two hemispheres and their oceanic counterparts. While it is commonly accepted that Termination I has been interrupted by a major cooling event (Younger Dryas (YD)) both in the Greenland (GRIP and GISP2) ice cores (Johnsen et al., 1992; Grootes et al., 1993) and in the oceanic records from the North Atlantic, the magnitude of a similar event (the Antarctic Cold Reversal, ACR) in East (Vostok, Dome B and Dome C) and West (Byrd Station) Antarctica ice cores (Jouzel et al., 1995; Blunier et al., 1998) seems to be much smaller. Moreover, the time relation between these two events is not yet settled. In fact, while the ACR in East Antarctica predates the YD from GRIP and GISP2 by more than 1 ka (Blunier et al., 1997), evidence from the Taylor Dome ice core (West Antarctica) seems to indicate that these events are synchronous between the two hemispheres (Steig et al., 1998). The YD/ACR events occur over very short time intervals (between 1 and 2 ka) and are therefore best documented, in the oceanic record, in high-resolution sediment cores.

Rapid climatic change is apparently not limited to D–O cycles during glacial time intervals and cooling events during terminations, but also affects interglacials. In fact, Greenland ice cores provide evidence for a very rapid Holocene

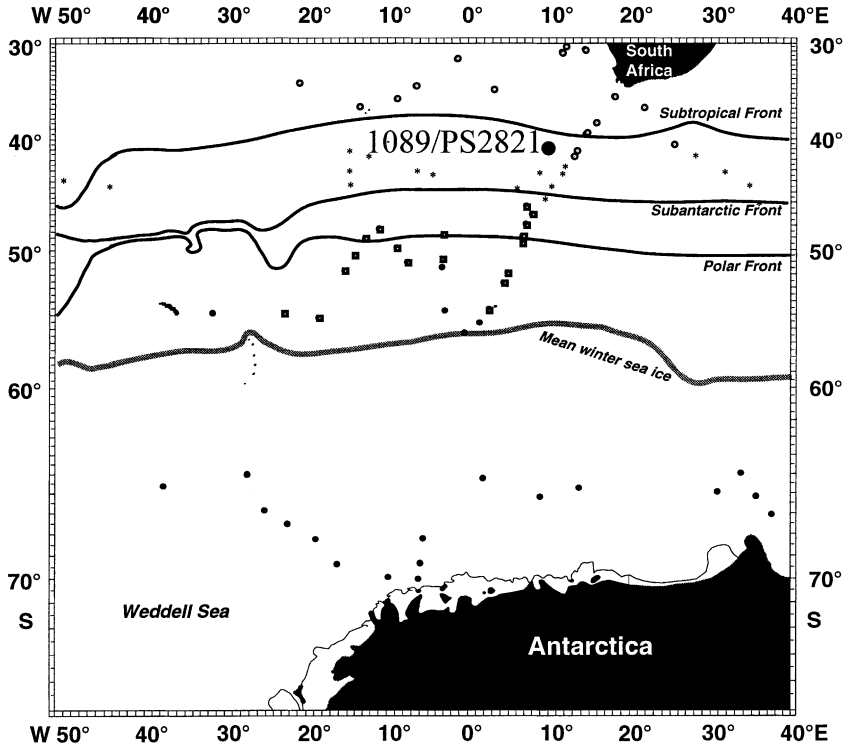

Fig. 1. Locations of ODP Site 1089 and Core PS2821-1 (large dot) and of the core-top samples used for the radiolarian reference database, in comparison to the average position of the oceanographic fronts (Peterson and Stramma, 1991), and the mean winter sea-ice distribution (Naval Oceanography Command Detachment, 1985). Different symbols have been assigned to stations according to which radiolarian assemblage reaches the higher factor component value at that station (also see Tables 2 and 3): factor 1 = filled circle, factor 2 = open circle, factor 3 = square, factor 4 = asterisk.

(MIS 1) cool and dry event at 8.2 ka (Alley et al., 1997; Mayewski et al., 1997; von Grafenstein et al., 1998), while an Eemian (MIS 5e) cooling event at ca. 122 ka has been recognized in European lakes (Field et al., 1994; Thouveny et al., 1994), Nordic Seas (Cortijo et al., 1994; Fronval and Jansen, 1996), Denmark shelf areas (Seidenkrantz et al., 1995) and the eastern South Atlantic (Maslin and Tzedakis, 1996; Maslin et al., 1998). Climatic variability during full interglacial conditions has also been demonstrated in the Southern Ocean (Pichon et al., 1992), and in a core from the Tasman Plateau (48°S), where alkenone SSTs indicate a mid-Eemian rapid cooling event at

Table 1
Tie-points between the different holes (A–D) at ODP Site 1089 used to produce the composite section (modified after Shipboard Scientific Party, 1999)

Sample	Depth (mbsf)	Depth (mcd)		Sample	Depth (mbsf)	Depth (mcd)
1089A, 1H-4, 140	5.90	5.66	tie to	1089D, 2H-2, 34	8.54	5.66
1089D, 2H-5, 136	14.06	11.18	tie to	1089A, 2H-3, 130	11.60	11.18
1089A, 2H-5, 112	14.42	14.00	tie to	1089B, 2H-3, 50	8.30	14.00
1089B, 2H-5, 140	12.20	17.90	tie to	1089D, 3H-4, 72	18.08	17.90
1089D, 3H-6, 54	20.90	20.72	tie to	1089B, 3H-1, 98	15.28	20.72
1089B, 3H-6, 76	22.56	28.00	tie to	1089C, 4H-1, 102	24.42	28.00

Table 2
Geographic location (latitude, longitude, water depth), sampling device (LBC = large box corer, MUC = multi-corer, MIC = micro-corer) and estimated SSST for the core tops in the reference dataset

Station	Latitude	Longitude	Water depth	Core type	SSST	Communality	Factor 1	Factor 2	Factor 3	Factor 4
PS1380-1	−70.007	−9.968	2072	LBC	−0.68	0.889	0.933	0.043	−0.128	−0.025
PS1386-1	−68.327	−5.616	4405	LBC	1.05	0.928	0.959	0.014	−0.065	−0.060
PS1387-1	−68.732	−5.837	2435	LBC	1.05	0.963	0.947	0.031	−0.255	−0.024
PS1394-1	−70.084	−6.681	1948	LBC	−0.59	0.802	0.855	0.021	−0.265	−0.002
PS1455-4	−65.417	1.833	2730	LBC	0.50	0.982	0.982	0.033	−0.123	−0.032
PS1751-2	−44.488	10.472	4770	MUC	9.75	0.926	0.074	0.342	−0.480	−0.757
PS1752-5	−45.620	9.608	4507	MUC	7.79	0.947	−0.012	0.226	−0.658	−0.680
PS1755-1	−47.788	7.102	4263	MUC	5.84	0.936	0.160	−0.010	−0.829	−0.473
PS1759-1	−50.153	5.755	3717	MUC	4.56	0.921	0.393	0.036	−0.871	−0.088
PS1765-1	−51.832	4.863	3749	MUC	2.93	0.882	0.475	0.005	−0.810	−0.023
PS1768-1	−52.592	4.460	3298	MUC	1.46	0.955	0.507	0.002	−0.835	−0.023
PS1771-4	−53.758	3.780	1811	MUC	0.44	0.878	0.352	0.008	−0.868	−0.024
PS1772-2	−55.458	1.167	4136	MUC	0.11	0.875	0.845	0.024	−0.399	−0.037
PS1773-2	−56.320	−0.480	3267	MUC	0.25	0.828	0.701	0.018	−0.579	−0.037
PS1774-1	−54.647	−2.870	2449	MUC	0.17	0.989	0.752	0.009	−0.648	−0.055
PS1775-5	−50.952	−7.502	2516	MUC	2.03	0.923	0.288	0.010	−0.915	−0.058
PS1776-6	−49.728	−8.768	3161	MUC	2.94	0.965	0.337	0.011	−0.913	−0.133
PS1777-7	−48.232	−11.037	2556	MUC	4.92	0.940	0.286	0.042	−0.913	−0.150
PS1778-1	−49.010	−12.703	3361	MUC	4.80	0.947	0.250	0.072	−0.924	−0.161
PS1779-3	−50.395	−14.075	3549	MUC	3.97	0.987	0.325	0.012	−0.932	−0.114
PS1780-1	−51.683	−15.273	4258	MUC	2.86	0.974	0.296	0.014	−0.939	−0.070
PS1782-6	−55.190	−18.610	5016	MUC	1.16	0.918	0.592	0.081	−0.748	−0.032
PS1783-2	−54.908	−22.718	3390	MUC	0.85	0.920	0.476	−0.021	−0.824	−0.117
PS1786-2	−54.932	−31.737	5756	MUC	1.40	0.832	0.753	0.031	−0.514	0.011
PS1805-5	−66.192	35.312	4149	MIC	0.49	0.782	0.834	0.010	−0.291	−0.023
PS1813-3	−64.955	33.628	2225	MIC	0.65	0.958	0.876	0.002	−0.429	−0.080
PS1821-5	−67.065	37.478	4028	MIC	0.17	0.866	0.839	−0.001	−0.391	−0.098
PS1823-1	−65.930	30.835	4442	MIC	0.36	0.799	0.852	−0.008	−0.263	−0.064
PS1825-5	−66.332	8.890	4341	LBC	0.36	0.933	0.926	0.016	−0.275	−0.008
PS1831-5	−65.743	13.657	2354	LBC	0.26	0.953	0.913	0.009	−0.329	−0.104
PS1957-1	−65.672	−37.478	4727	MIC	−0.57	0.945	0.915	0.016	−0.308	−0.107
PS1967-1	−65.957	−30.071	4847	MIC	−0.42	0.892	0.933	0.046	−0.142	−0.017
PS1973-1	−66.891	−25.548	4841	MIC	0.13	0.948	0.934	0.028	−0.270	−0.032
PS1975-1	−67.508	−22.522	4893	MIC	0.30	0.851	0.887	0.004	−0.230	−0.112
PS1977-1	−68.284	−19.340	4838	MIC	−0.05	0.790	0.879	0.017	−0.044	−0.126
PS1979-1	−69.367	−16.497	4735	MIC	−0.22	0.959	0.975	0.028	−0.059	−0.064
PS2073-1	−39.590	14.566	4692	MUC	17.27	0.930	−0.018	0.921	−0.058	−0.280
PS2076-1	−41.135	13.481	2086	MUC	15.08	0.787	−0.035	0.773	0.028	−0.433
PS2080-1	−41.717	13.047	5078	MUC	12.63	0.758	0.055	0.617	−0.193	−0.580
PS2081-1	−42.692	12.191	4794	MUC	10.87	0.925	−0.020	0.401	−0.301	−0.820
PS2082-3	−43.218	11.759	4661	MUC	10.87	0.907	0.038	0.512	−0.277	−0.752
PS2083-2	−46.370	7.036	1955	MUC	8.14	0.892	−0.063	0.123	−0.862	−0.360
PS2084-2	−47.024	7.959	1664	MUC	6.80	0.954	0.206	0.012	−0.934	−0.198
PS2087-1	−49.134	6.706	3451	MUC	4.99	0.979	0.202	0.019	−0.961	−0.118
PS2103-2	−51.330	−3.324	2947	MUC	3.80	0.831	0.673	0.100	−0.583	−0.169
PS2104-2	−50.742	−3.212	2592	MUC	2.35	0.879	0.475	−0.004	−0.807	−0.031
PS2105-2	−48.694	−2.848	3618	MUC	4.60	0.955	0.171	0.047	−0.948	−0.161
PS2109-3	−35.000	3.167	5041	MUC	18.20	0.820	0.048	0.860	0.027	−0.279
PS2254-1	−43.973	−50.073	5341	MUC	14.19	0.857	0.267	0.560	−0.301	−0.618
PS2256-4	−44.513	−44.465	5111	MUC	12.00	0.865	0.173	0.284	−0.026	−0.868
PS2487-2	−35.827	18.107	2942	MUC	20.28	0.928	0.025	0.870	0.034	−0.411
PS2488-1	−38.557	15.802	4888	MIC	18.70	0.865	−0.026	0.779	−0.003	−0.508

Table 2
Geographic location (latitude, longitude, water depth), sampling device (LBC = large box corer, MUC = multi-corer, MIC = micro-corer) and estimated SSST for the core tops in the reference dataset

Station	Latitude	Longitude	Water depth	Core type	SSST	Communality	Factor 1	Factor 2	Factor 3	Factor 4
PS2489-4	−42.887	8.982	3795	MUC	12.04	0.940	0.044	0.411	−0.098	−0.871
PS2491-4	−44.955	5.970	4323	MUC	9.32	0.860	0.026	0.226	−0.288	−0.852
PS2492-1	−43.175	−4.052	4197	MUC	11.81	0.943	−0.011	0.396	−0.013	−0.886
PS2493-3	−42.883	−6.020	4174	MUC	12.02	0.969	−0.020	0.392	−0.067	−0.901
PS2494-1	−41.690	−12.340	3324	MUC	14.44	0.877	0.128	0.583	0.072	−0.719
PS2495-1	−41.288	−14.500	3135	MIC	14.67	0.847	0.015	0.597	0.027	−0.700
PS2496-2	−43.010	−14.608	3518	MUC	13.62	0.834	0.066	0.440	−0.116	−0.789
PS2498-2	−44.153	−14.228	3782	MUC	10.98	0.881	−0.049	0.322	−0.116	−0.873
PS2557-2	−36.920	21.825	3371	MUC	21.70	0.934	−0.010	0.931	0.016	−0.256
PS2560-3	−40.537	25.568	2641	MUC	19.35	0.951	0.106	0.926	−0.018	−0.287
PS2561-1	−41.860	28.547	4471	MUC	15.46	0.934	0.079	0.577	−0.033	−0.770
PS2562-1	−43.183	31.577	5193	MIC	11.69	0.916	0.020	0.585	−0.143	−0.744
PS2563-3	−44.550	34.783	3515	MUC	11.26	0.955	0.190	0.323	−0.194	−0.881
PS2564-2	−46.142	35.900	3035	MUC	9.03	0.941	0.199	0.214	−0.368	−0.848
GeoB2004-1	−30.868	14.342	2569	MUC	18.96	0.883	0.020	0.876	0.006	−0.338
GeoB2007-1	−30.438	12.155	3906	LBC	20.04	0.859	−0.008	0.883	0.010	−0.282
GeoB2008-1	−31.102	11.715	4312	LBC	20.60	0.930	0.043	0.873	0.021	−0.408
GeoB2016-3	−31.905	−1.303	3385	MUC	21.71	0.854	0.014	0.923	−0.001	−0.051
GeoB2018-1	−34.662	−6.563	4241	MUC	19.29	0.889	−0.002	0.926	−0.006	−0.180
GeoB2019-2	−36.053	−8.767	3825	MUC	18.56	0.934	0.079	0.884	0.041	−0.381
GeoB2021-4	−36.833	−14.403	3575	MUC	19.11	0.898	−0.014	0.911	−0.019	−0.259
GeoB2022-3	−34.438	−20.885	4025	MUC	19.63	0.942	−0.009	0.957	−0.006	−0.160
						Variance	26.126	21.066	24.178	19.021
						Cumulative variance	26.126	47.192	71.369	90.390

For each sample the communality, the varimax factor component and the percent of the total information explained (along with its corresponding cumulative value) for the first four factors are also shown.

around 120 ka, possibly a Southern Ocean event (Ikehara et al., 1997). However, the geographical extent of these events is still not clear, with debate continuing on whether they were of regional or global significance.

In this paper we therefore address the following questions:

– Are the D–O cycles recognizable in the SSST signal of the Southern Ocean? Which mechanisms (thermohaline oceanic or atmospheric circulation changes) are driving these variations?

– Is it possible to recognize sudden cooling events such as the YD and the ACR in the sedimentary record of the Southern Ocean? Did these events occur at both Terminations I and II?

– How stable are climatic optima (MIS 1 and 5e) in the Southern Ocean? Is there evidence of sudden changes during these generally warm time intervals?

2. Materials and methods

2.1. Cores and sample preparation

ODP Site 1089 (ODP Leg 177) and piston Core PS2821-1 (R/V '*Polarstern*' cruise ANT XIV/3) are located at the South Atlantic STF (40°56′S; 9°54′E, 4620 m water depth and 40°57′S; 9°53′E, 4575 m water depth, respectively, Fig. 1). ODP Site 1089 was sampled in four holes (A–D), which were correlated by means of the down core changes in magnetic susceptibility, color reflectance and γ-ray attenuation bulk density measurements (Shipboard Scientific Party, 1999). Details of the measured physical properties, as well as the tie-points between cores sampled at different holes, can be found in Shipboard Scientific Party, 1999: figs. 14–16 and tables 4 and 5, respectively. In the present work we used the top 7.94 m of

Core PS2821-1 together with a 16.17-m-long portion of the composite record of ODP Site 1089: from sample 1089D, 2H-4, 0–2 cm = 8.32 mcd (meters composite depth), to sample 1089B, 3H-3, 140–142 cm = 24.49 mcd (Table 1).

Core PS2821-1 and the composite section of ODP Site 1089 were correlated by means of their color reflectance, magnetic susceptibility and *Cycladophora davisiana* relative abundance changes records. The tie-point is at 7.94 m depth in Core PS2821-1, corresponding to 8.34 mcd at ODP Site 1089. For details on the development of the age model for PS2821-1, see 2.4. Age model.

A total of 271 levels in the cores were sampled at 10-cm intervals, which was switched to 5-cm intervals close to Terminations I and II.

Both age model- and sampling depths-related data are available at http://www.pangaea.de.

Radiolarian slides were prepared according to standard laboratory techniques (Abelmann et al., 1999). A Zeiss Axioskop microscope, at 160× magnification, was used for determining the relative abundance of radiolarian species. An average of 479 specimens were counted for each slide.

2.2. Paleotemperatures

For the paleotemperature estimations at Site 1089 and PS2821-1, 20 additional surface samples were collected during R/V '*Polarstern*' (ANT X/5, XI/2, XI/4) and R/V '*Meteor*' (M23/1) cruises, to extend the available core-top reference dataset for the Southern Ocean (Abelmann et al., 1999), by using a large box corer (LBC) and a multiple corer (MUC).

The reference dataset (Fig. 1, Tables 2 and 3) thus includes 73 stations, extends to the Subtropical area (30°S), and documents the whole paleotemperature fluctuations between the Antarctic and Subtropical regimes.

A total of 252 radiolarian taxa (most of them at a species or subspecies level) have been recognized in this study. The baselines for defining the reference dataset (Abelmann et al., 1999) led to a suit of 24 taxa (Table 4, Plates I and II), including warm water-adapted species from the Subtropical area.

Ocean temperature data were obtained from the Southern Ocean Atlas (Olbers et al., 1992) and the World Ocean Atlas 1994 (Levitus and

Table 3
Overview of the radiolarian assemblages recognized in the core-top dataset

Radiolarian assemblages	Temperature range	Latitude range	Taxa
Southern Antarctic Zone (F1) assemblage ●	−1–2°C	55–70°S	*Spongotrochus glacialis* *Actinomma leptoderma* *Saccospyris antarctica* *Phormospyris stabilis antarctica*
Antarctic/Polar Front Zone (F3) assemblage ■	0–8°C	46–55°S	*Phorticium clevei* *Actinomma antarcticum* *Phormospyris stabilis antarctica* *Saccospyris antarctica*
Subantarctic Zone assemblage (F4) *	8–16°C	41–46°S	*Lithomelissa boreale* *Eucecryphalus gegenbauri* *Saccospyris inflata* *Lithomelissa thoracites*
Subtropical assemblage (F2) ○	14–22°C	30–41°S	*Collosphaera* spp. *Tetrapyle octacantha* *Carpocanistrum* spp. *Eucyrtidium* spp. *Lithomelissa thoracites* *Pterocorys clausus/zancleus* *Hymeniastrum* spp.

The factor names, the temperature and latitudinal ranges, as well as the taxa having varimax factor scores higher than 1, are indicated for each factor. The symbols below the assemblage names correspond to those shown in Fig. 1.

Table 4
Scaled varimax factor scores matrix (species vs. factor scores) for the 24 species used in the reference dataset

Species	Factor 1	Factor 2	Factor 3	Factor 4
Actinomma antarcticum	−0.680	0.186	**−2.675**	0.395
Actinomma leptoderma	**2.675**	0.188	0.787	−0.636
Carpocanistrum spp.	−0.039	**1.543**	−0.057	0.458
Collosphaera spp.	−0.026	**2.193**	−0.134	0.939
Corocalyptra columba	−0.008	0.620	−0.023	0.281
Didymocyrtis tetrathalamus	−0.015	0.962	−0.051	0.457
Eucecryphalus gegenbauri	−0.024	0.290	0.209	**−1.528**
Eucyrtidium spp.	0.003	**1.509**	0.132	−0.536
Heliodiscus asteriscus	−0.013	0.421	−0.016	0.044
Hymeniastrum spp.	−0.005	**1.188**	0.089	−0.242
Larcopyle bütschlii	−0.061	0.847	0.007	−0.348
Lithomelissa boreale	−0.098	−0.611	0.311	**−3.667**
Lithomelissa thoracites	−0.041	**1.422**	0.162	**−1.149**
Peromelissa phalacra	0.000	0.630	−0.006	0.216
Phormospyris stabilis antarctica	**1.558**	0.247	**−1.243**	0.476
Phorticium clevei	−0.226	−0.29	**−3.609**	−0.995
Pterocorys clausus/zancleus	−0.068	**1.378**	0.035	−0.408
Saccospyris antarctica	**2.193**	0.101	**−1.058**	0.350
Saccospyris inflata	−0.250	0.368	−0.515	**−1.483**
Spongocore puella	0.018	0.571	0.030	0.112
Spongotrochus glacialis	**2.999**	−0.138	−0.196	−0.224
Stylochlamydium asteriscus	−0.004	0.707	−0.013	0.132
Theocorythium trachelium	0.002	0.746	0.080	−0.186
Tetrapyle octacantha	−0.122	**2.092**	−0.091	−0.786

Absolute values higher than 1.000 have been highlighted (bold).

Boyer, 1994). Data from this latter source have been extracted using the program Ocean Data View (Schlitzer, 2000). The temperature data represent austral SSSTs, averaged from December to March at 10 m water depth. SSSTs have been used because sediment trap studies from the Southern Ocean have demonstrated that more than 90% of the annual radiolarian flux from the surface waters to the sediment occurs in this season (Abelmann and Gersonde, 1991; Abelmann, 1992). Further baselines for choosing the hydrographic data are described elsewhere (Abelmann et al., 1999).

The CABFAC, THREAD and REGRESS routines of the Imbrie and Kipp method (IKM) for Q-mode factor analysis were run using the PaleoToolBox and MacTransfer software packages (Sieger et al., 1999). The log-transformed surface reference dataset was resolved by a Q-mode factor analysis in four varimax factors (Tables 2–5), which explain 90.39% of the total data information. A stepwise multiple-regression analysis was used to define a transfer function. The goodness of fit for the calibration equation (Fig. 2) is $r = 0.992$ (0.990, when adjusted for degrees of freedom), giving a corresponding standard error of estimate of ± 1.053°C (with a corrected value of ± 1.161°C). Most of the residuals (estimated minus measured temperature values) are within one standard deviation (Fig. 2), and the absolute value of only two residuals is higher than 2°C. The scaled varimax factor scores and components, along with the coefficients for each term in the regression equation, are reported in Tables 2, 4 and 5. A summary of the assemblages is shown in Table 3 and Fig. 1.

2.3. Spectral analysis

A non-parametric multi-taper method, MTM (Thomson, 1982), was used for spectral analysis, as it provided high spectral resolution even for short time series, and statistical confidence levels (F-test) for the validity of location of each peak in

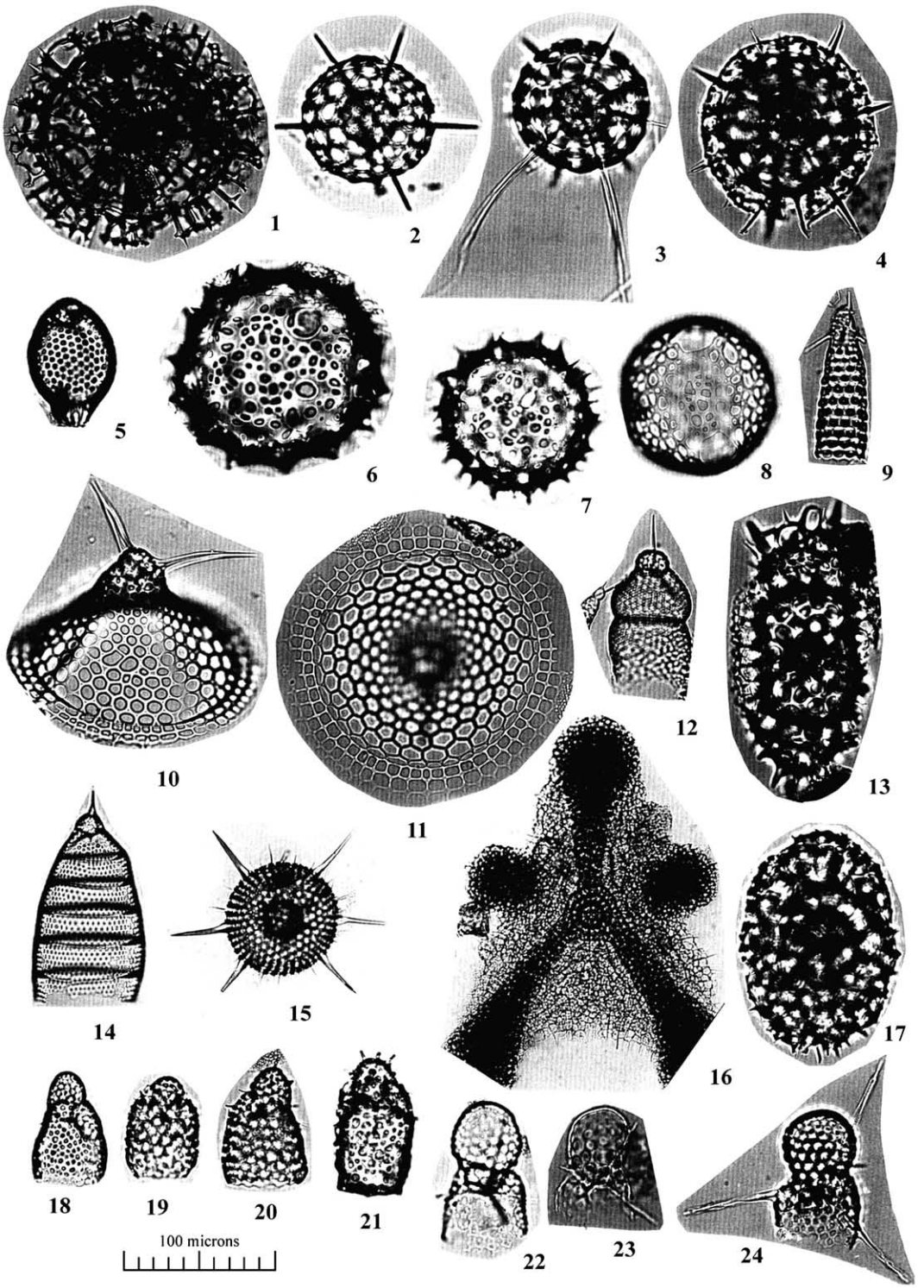
1
2
3
4
5
6
7
8
9
10
11
12
13
14
15
16
17
18
19
20
21
22
23
24
100 microns

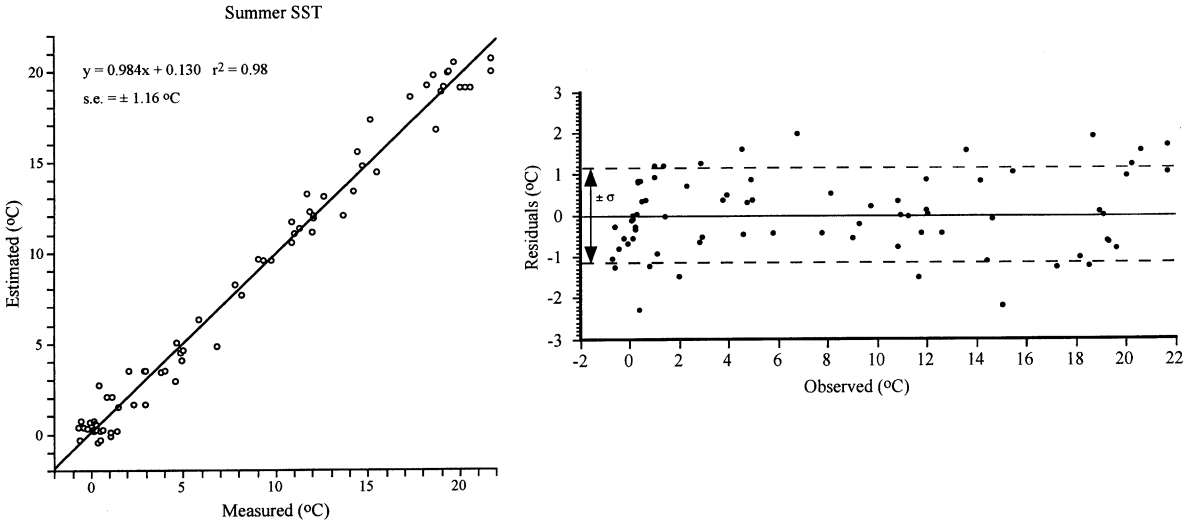

Fig. 2. Observed versus estimated mean summer SST (December to March) for all core tops included in the reference database. Indicated are the linear regression line, equation and standard error of estimate. Observed summer SST versus residual for SST with $\pm\sigma$ (one standard deviation).

Plate I. Scale bar = 100 μm for all figures, except figs. 1 and 15 (scale bar = 200 μm). All samples are core tops, unless otherwise indicated.

1 *Actinomma antarcticum* (Haeckel), GeoB2021
2 *Actinomma leptoderma leptoderma* (Jørgensen), GeoB2019
3 *Actinomma leptoderma* (Jørgensen) *longispina* Cortese and Bjørklund, GeoB2016
4 *Actinomma boreale* Cleve, GeoB2007
5 *Carpocanistrum* spp., GeoB2007
6 *Collosphaera* spp., GeoB2007
7 *Collosphaera* spp., GeoB2016
8 *Collosphaera* spp., GeoB2016
9 *Artostrobus annulatus* (Bailey), PS2498
10 *Eucecryphalus gegenbauri* Haeckel, PS2489
11 *Eucecryphalus gegenbauri* Haeckel, apical view, PS2259
12 *Corocalyptra columba* (Haeckel), GeoB2019
13 *Didymocyrtis tetrathalamus tetrathalamus* (Haeckel), PS2487
14 *Eucyrtidium* spp., GeoB2016
15 *Heliodiscus asteriscus* Haeckel, GeoB2016
16 *Hymeniastrum* spp., PS2487
17 *Larcopyle bütschlii* Dreyer, PS2489
18 *Lithomelissa boreale* (Ehrenberg), PS2498
19 *Lithomelissa hystrix* Jørgensen, PS2498
20 *Lithomelissa* (?) sp. A Petrushevskaya, PS2259
21 *Lithomelissa* (?) sp. A Petrushevskaya, PS2259
22 *Lithomelissa thoracites* Haeckel, GeoB2010
23 *Lithomelissa thoracites* Haeckel, GeoB2010
24 *Lithomelissa thoracites* Haeckel, Core 1089B, 5H-2, 110–112 cm

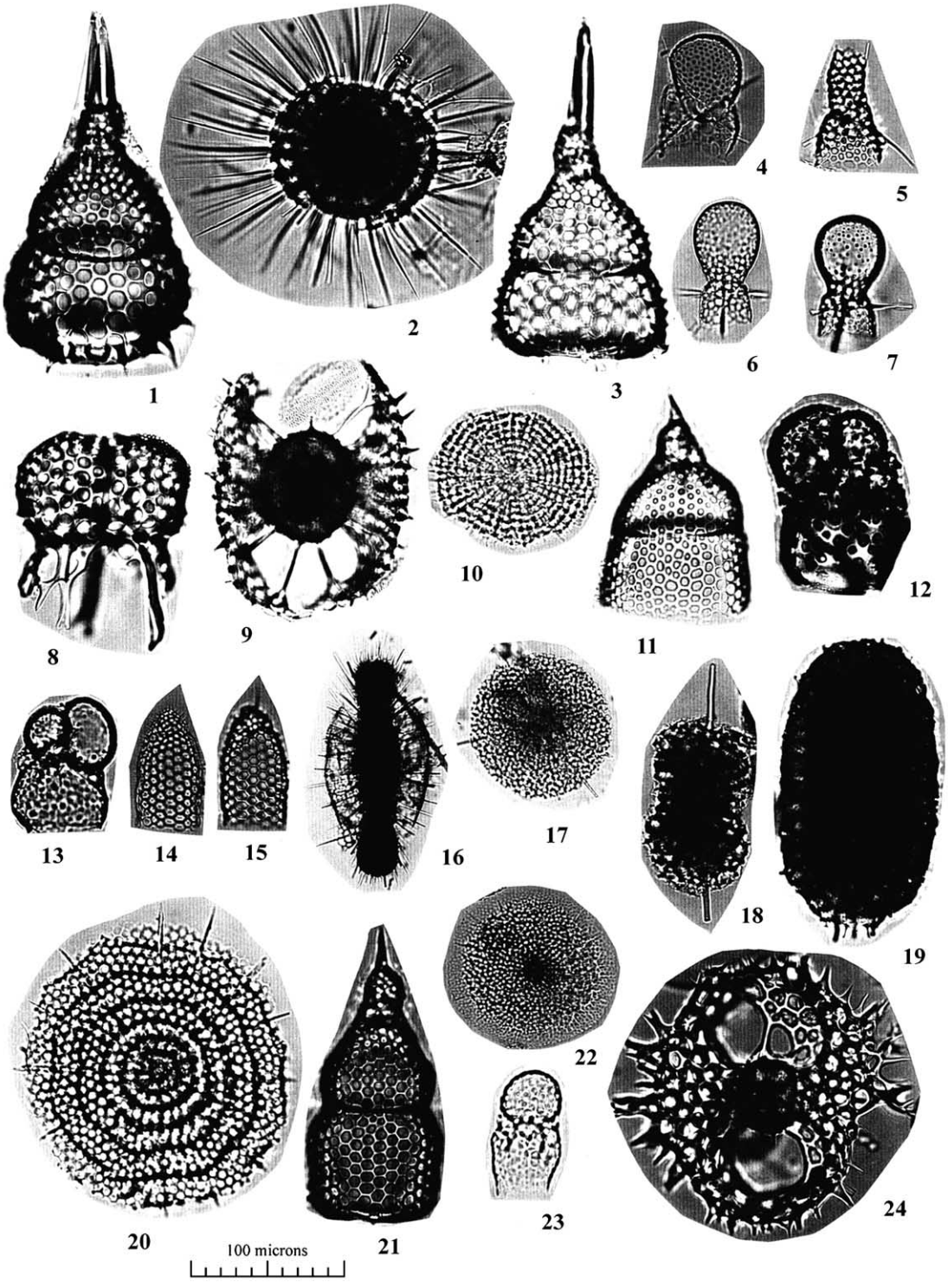
1
2
3
4
5
6
7
8
9
10
11
12
13
14
15
16
17
18
19
20
21
22
23
24
100 microns

the spectrum and its amplitude (thus providing a high degree of confidence for low amplitude oscillations not spotted by other methods). It was therefore preferred to the classical Blackman–Tuckey method, which has a poor spectral resolution and where the statistical significance of a peak is highly correlated to its amplitude (Thomson, 1982). As the orbitally related spectral peaks usually have larger amplitudes than the high-frequency peaks, in a short record the high-frequency signal will be drowned by the signal connected to the low frequencies. In order to minimize this problem, the low-frequency components are removed by pre-whitening (high-pass filter, pre-whitening constant of 0.5) before proceeding to the application of MTM.

2.4. Age model

The final age model for both cores was developed using the following steps:

(a) the isotopic record of benthic foraminifera and its age interpretation (Mortyn et al., submitted) according to the SPECMAP chronology (Martinson et al., 1987) provided a preliminary depth-to-age relation for Core 1089;

(b) cores 1089 and PS2821-1 were correlated based on magnetic susceptibility and color reflectance (red band, 650–750 nm);

(c) the previous two steps were integrated to provide a depth-to-age relation for PS2821-1;

(d) the preliminary age assignments for the two cores were then fine-tuned based on *Cycladophora davisiana* relative percentage changes, which were compared to the corresponding record from RC11-210 (Martinson et al., 1987), thus providing additional depth–age information.

Data relevant to points (b) and (d) above are available at http://www.pangaea.de.

3. Results

3.1. Paleotemperatures

The paleotemperature reconstruction (Figs. 3–

Plate II. Scale bar = 100 μm for all figures, except figs. 16, 17 and 22 (scale bar = 200 μm). All samples are core tops, unless otherwise indicated.

1 *Lamprocyclas maritalis* Haeckel, GeoB2007
2 *Lithelius minor* Jørgensen, GeoB2019
3 *Lamprocyclas maritalis* Haeckel, GeoB2019
4 *Lithomelissa* (?) *laticeps* Jørgensen, Core 1089C, 4H-4, 100–102 cm
5 *Lophophaena bütschlii* (Haeckel), GeoB2007
6 *Peromelissa phalacra* (Haeckel), GeoB2016
7 *Peromelissa phalacra* (Haeckel), GeoB2016
8 *Phormospyris stabilis* (Goll) *antarctica* (Haecker), PS2259
9 *Phorticium clevei* (Jørgensen), PS2259
10 *Porodiscus* sp. 2, Core 1089C, 4H-4, 100–102 cm
11 *Pterocorys clausus* (Popofsky)/*Pterocorys zancleus* (Müller), PS2489
12 *Saccospyris antarctica* Haecker, PS2259
13 *Saccospyris inflata* (Bailey), PS2489
14 *Sethoconus* (?) *tabulatus* (Ehrenberg), GeoB2016
15 *Sethoconus* (?) *tabulatus* (Ehrenberg), GeoB2016, same specimen, different focus level
16 *Spongocore puella* Haeckel, M2016
17 *Spongotrochus glacialis* Popofsky, PS2491
18 *Spongurus* (?) sp. Petrushevskaya, PS2259
19 *Spongurus pylomaticus* Riedel, PS2491
20 *Stylochlamydium asteriscus* Haeckel, GeoB2016
21 *Theocorythium trachelium* (Ehrenberg), GeoB2021
22 *Stylochlamydium venustum* Bailey, Core 1089C, 4H-4, 100–102 cm
23 *Trisulcus testudus* Petrushevskaya, Core 1089C, 4H-4, 100–102 cm
24 *Tetrapyle octacantha* Müller, PS2491

Table 5
Statistical summary of the first seven factors extracted by the program CABFAC: eigenvalue and cumulative variance explained (top)

Factor	Eigenvalue	Cumulative variance
1	33.04	44.65
2	21.73	74.02
3	8.13	85.01
4	3.98	90.39
5	1.62	92.58
6	1.08	94.04
7	0.92	95.29
	Regression term	Regression coefficient
	F1sq	13.07
	F2sq	5.99
	F3sq	4.13
	F4sq	5.77
	F1*F2	29.09
	F1*F3	−9.84
	F1*F4	−19.45
	F2*F3	8.82
	F2*F4	−3.13
	F3*F4	8
	F1	−27.44
	F2	2.98
	F3	9.97
	F4	9.65
	Intercept	13.16

Regression terms (radiolarian assemblages/factors) and coefficients for the paleotemperature regression equation (bottom).

5) shows temperature fluctuations of a few degrees around 13°C in MIS 6 (Figs. 3A and 4D). A sudden warming transition from cold to interglacial temperatures occurs over a few ka, reaching a maximum temperature of 19°C (ca. 3°C warmer than present temperature, i.e. 15.8°C, at the core location) at 128 ka. Within this warming trend, two short cooling events, with a temperature decrease of 2–3°C, are centered at 130–131 and at 132–133 ka (Fig. 4D). Temperatures then steadily decrease, reaching glacial values of ca. 13°C by 114 ka (i.e. a few kyr after the 5e/5d boundary). MIS 5e is marked by three major (ca. 3°C) cooling trends, reaching minimum temperatures at 124, 118 and 114 ka (Fig. 3A). In MIS 5c and 5a warmest temperatures of ca. 17°C occur at about 105 and 84 ka, separated by a temporary cooling (to 13°C, centered at 90 ka) during substage 5b (Fig. 3A). The transition from MIS 5 to 4, at 74 ka, marks the beginning of a different mode of climatic variability, characterized by short-term temperature oscillations of about 3–4°C amplitude, lasting a maximum of a few thousand years. Coldest temperatures (ca. 11°C) are reached between 17 and 28 ka in MIS 3 and 2. These temperatures are ca. 1°C colder than the minimum temperatures recorded during MIS 6.

At Termination I (Figs. 3C and 4C), a temperature increase of about 6–7°C leads to Holocene conditions with temperatures up to 17–18°C at 11 ka. This warming is interrupted by two short-term cooling events (of ca. 2°C) at 12.3 and 11.2 ka. The warm temperatures at 11 ka are followed by a cold event reaching minimum temperatures (just below 15°C) at 9 ka and a warm event (slightly above 17°C) centered at ca. 7 ka. This temperature change spans a time period of ca. 10 ka, with a total warming of ca. 7°C.

This evolution is almost identical to that observed at Termination II (Fig. 4D): at 140 ka, the temperature is at a glacial minimum in MIS 6 and, after a relatively weak warming trend occurring over 8 ka, another relative minimum is

Fig. 3. (A) Down core SSST over the past 160 ka at ODP Site 1089 and PS2821, and $\delta^{18}O$ PDB variations for the planktic foraminifer *Globigerina bulloides* (Mortyn et al., submitted) at ODP Site 1089. The age model for ODP Site 1089 and PS2821-1 is the one developed in this paper (see 2.4. Age model). The dashed line represents today's temperature (15.8°C) at the core location. The topmost bar includes the MIS 1–6, with their age according to Martinson et al. (1987). (B) Changes over the past 40 ka in CH_4 concentrations (in parts per billion in volume) for gas trapped in air bubbles in the GRIP ice core (Greenland). CH_4 data and the gas-age model for this core are from Chappellaz et al. (1993). Vertical dashed lines mark the position of quasi-synchronous climatic changes. Interstadials 5–8 and 10–11 are the same as those recognized when comparing the CH_4 and the $\delta^{18}O$ record in the GRIP ice core (Chappellaz et al., 1993). (C) Paleotemperature record at PS2821-1. (D) Paleotemperatures above the atmospheric inversion layer at Vostok Station (Antarctica), given as a difference from today's value (Petit et al., 1999). The age model for the Vostok ice core is from Petit et al. (1999). The age assignment of some of the most prominent climatic changes during MIS 5 (Fig. 3A) discussed in the text, as well as the approximate location of the YD-I ('YD-type') and the ACR-I ('ACR-type') cooling events (Fig. 3C) are reported for clarity. Note the change in age scale between A and B–D.

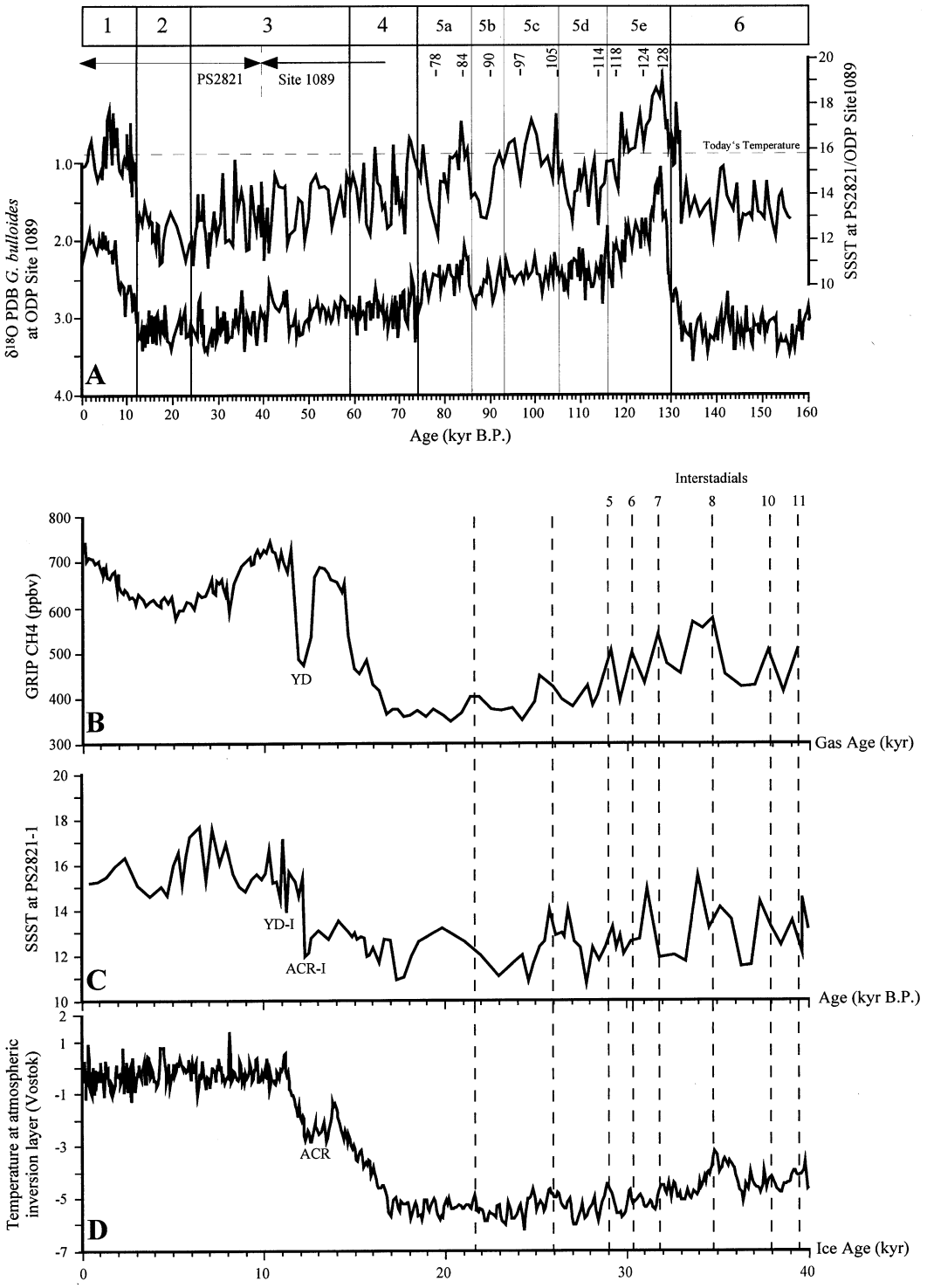
1
2
3
4
5a
5b
5c
5d
5e
6
PS2821
Site 1089
-78
-84
-90
-97
-105
-114
-118
-124
-128
Today's Temperature
δ18O PDB G. bulloides at ODP Site 1089
SSST at PS2821/ODP Site1089
A
Age (kyr B.P.)
Interstadials
5
6
7
8
10
11
GRIP CH4 (ppbv)
YD
B
Gas Age (kyr)
SSST at PS2821-1
YD-I
ACR-I
C
Age (kyr B.P.)
Temperature at atmospheric inversion layer (Vostok)
ACR
D
Ice Age (kyr)

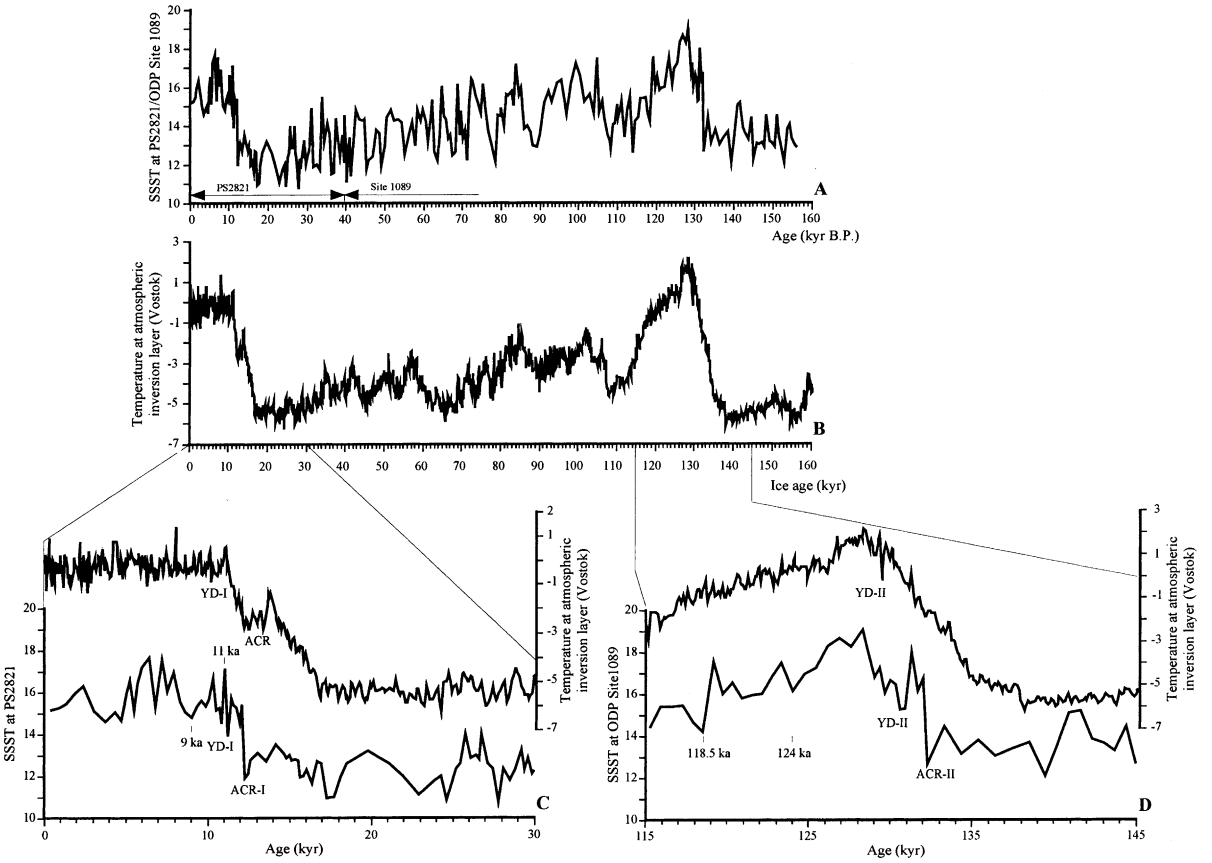

Fig. 4. Comparison of paleotemperature changes at PS2821/ODP Site 1089 and at Vostok Station, Antarctica. The age model and temperature data for Vostok are from Petit et al. (1999). (A) SSST record for PS2821/ODP Site 1089. (B) Atmospheric paleotemperatures at the inversion layer reconstructed from the Vostok ice core (Antarctica), given as a difference from today's value (Petit et al., 1999). (C) Blow-up of A and B for a 30-kyr interval including Termination I. The positions of the cooling events recognized at this termination in the SSST record of PS2821 are reported as YD-I and ACR-I. For the Vostok ice core, the position of the ACR and of an event similar to YD-I are also shown. (D) Same as above, for Termination II. The positions of the cooling events recognized at this termination in the SSST record of Site 1089 are reported as YD-II and ACR-II. For the Vostok ice core, the position of an event similar to YD-II is also shown.

reached at 132 ka. At this time the major transition takes place, with a warming of 5.5°C. This relative temperature maximum is followed by a short climatic deterioration, with temperatures almost 3°C cooler at 130–131 ka. Another climatic rebound follows, with an absolute warm peak at 128 ka in MIS 5e. This evolution takes place over 12 ka and the total warming is 7°C.

Fig. 5. Physical properties, isotopic and paleotemperature records for ODP Site 1089 and Core PS2821-1 over the past 160 ka. Magnetic susceptibility and color reflectance measurements from Shipboard Scientific Party (1999). Age assignment of MIS 1–6 after Martinson et al. (1987). The arrows and dashed line in E and F identify the portions of these records belonging to Core PS2821-1 and to ODP Site 1089. (A) Smoothed color reflectance (percentage of reflected to incoming radiation) in the 550–650-nm band for ODP Site 1089. (B) Color reflectance (percentage of reflected to incoming radiation) in the 550–650-nm band for Core PS2821-1. (C) Magnetic susceptibility ($SI \times 10^{-5}$ units) for ODP Site 1089. (D) Magnetic susceptibility ($SI \times 10^{-5}$ units) for Core PS2821. (E) Changes in the relative abundance of *Cycladophora davisiana* along the PS2821-1/ODP Site 1089 record. (F) Estimated IKM-radiolarian SSST for the PS2821-1/ODP Site 1089 record. (G) $\delta^{18}O$ PDB for the planktic foraminifer *Globigerina bulloides* (Mortyn et al., submitted).

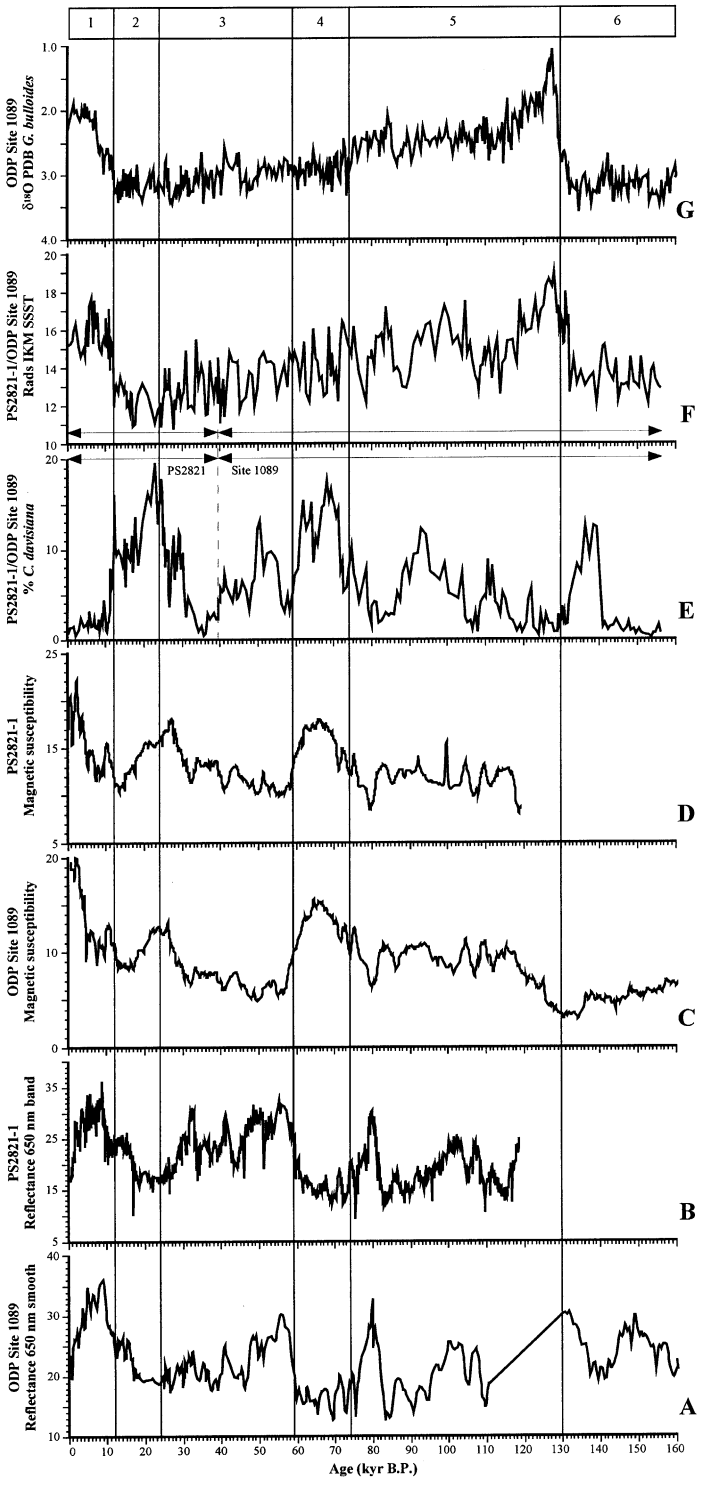
1
2
3
4
5
6
ODP Site 1089
δ18O PDB G. bulloides
G
PS2821-1/ODP Site 1089
Rads IKM SSST
F
PS2821
Site 1089
PS2821-1/ODP Site 1089
% C. davisiana
E
PS2821-1
Magnetic susceptibility
D
ODP Site 1089
Magnetic susceptibility
C
PS2821-1
Reflectance 650 nm band
B
ODP Site 1089
Reflectance 650 nm smooth
A
Age (kyr B.P.)

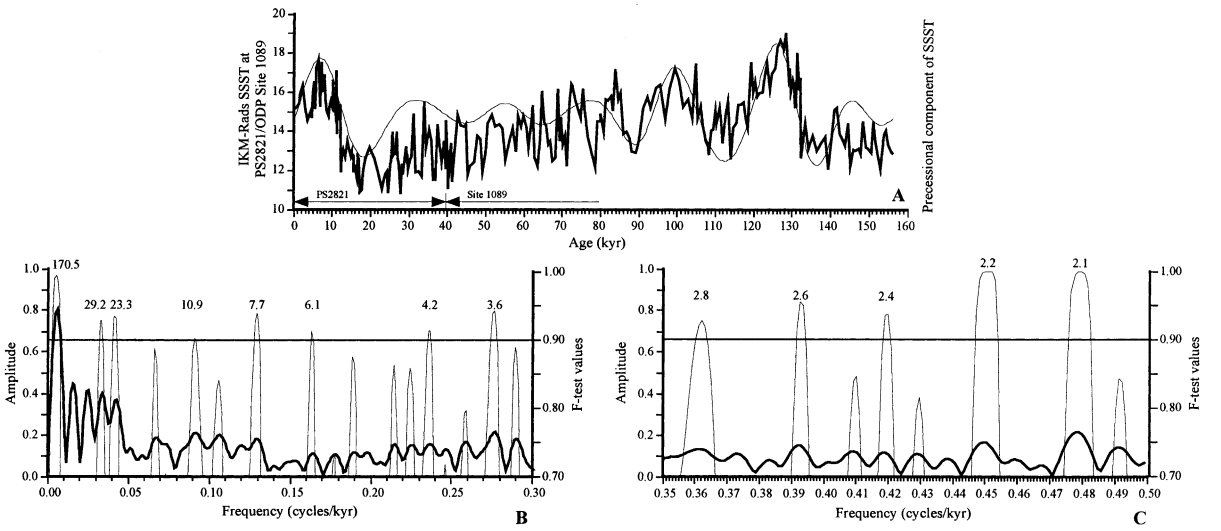

Fig. 6. (A) The paleotemperature record of ODP Site 1089 and Core PS2821-1 for the last 160 ka compared to its precessional component (thin line). (B,C) The results of MTM spectral analysis for the paleotemperature record, together with the frequency, amplitude and *F*-test values (thin line) for the spectra. The periods for spectral peaks with an *F*-test value higher than 0.90 (see Table 6) are also shown. Note the change in scale for the frequency axis between B and C.

3.2. Spectral analysis

The detailed sampling interval (Δ = ca. 0.6 kyr) available for our cores makes it possible to perform spectral analysis of the SSST signal for frequencies between 0 and 0.5 cycles/kyr, as the Nyquist frequency ($f_N = 1/2\Delta$, the highest detectable frequency for data sampled at intervals Δ) of our time series is 0.83 cycles/kyr, and therefore higher than 0.5 cycles/kyr. Moreover, the high sedimentation rate (generally more than 0.15 m/kyr) strongly reduces the possible smearing of the signal by bioturbation, a process which usually operates on thicknesses of a few cm.

We were able to document the presence of spectral peaks (with *F*-test confidence levels higher than 0.90, Fig. 6, Table 6) at frequencies close to the orbital peaks, but shifted towards higher frequency values. The first detected peak is at a frequency of 0.006 cycles/kyr (period of 170.5 ka) and is not connected to the eccentricity cycle, but to the short length of the record (Winograd et al., 1988; Yiou et al., 1991). The absence of an obliquity spectral signature (in contrast to its presence in Vostok) is to be expected, as our cores are located at a much lower latitude (40°S instead of 78°S) than Vostok, and therefore the influence of the obliquity forcing is subdued (i.e. at these latitudes it is not the yearly amount of heat received that is important, but rather its partition-

Table 6
Statistically significant (*F*-test value >0.90) spectral peaks obtained by an MTM applied to the paleotemperature record

Frequency	Period	Amplitude	*F*-test
0.006	170.5	0.804	0.994
0.034	29.2	0.398	0.929
0.043	23.3	0.366	0.932
0.092	**10.9**	0.209	0.903
0.130	7.7	0.178	0.940
0.164	**6.1**	0.110	0.913
0.237	**4.2**	0.154	0.914
0.278	**3.6**	0.210	0.943
0.319	3.1	0.183	0.996
0.362	**2.8**	0.129	0.928
0.392	2.6	0.148	0.956
0.419	**2.4**	0.112	0.937
0.450	2.2	0.165	0.999
0.479	2.1	0.214	0.999

The frequency (in cycles/kyr), period (in kyr), amplitude and *F*-test value are reported for each peak. The bold values correspond to periodicities close to those recognized in the Vostok ice-core record (Yiou et al., 1991).

ing through the year). The importance of the precessional forcing at our core location can already be recognized by the close match between the paleotemperature signal and its precessional filtered component (Fig. 6A). The differences in these two curves (from 20 to 70 ka) arise from higher frequency responses of the climatic system to the orbital forcing (see 4.4. Spectral analysis, high-frequency non-linear climatic responses to orbital forcing, and internal mechanisms). The precessional forcing is identified by the two next significant peaks, located at 0.034 and 0.043 cycles/kyr (periods of 29.2 and 23.3 ka, respectively). The operation of non-linear processes can be identified by examining high-frequency spectra of climatic proxies, as the climatic system responds to orbital forcing by generating harmonics and combination tones of the forcing frequencies. In our record, the positions of the spectral peaks for these higher frequencies are at 10.9, 6.1, 4.2, 3.6, 2.8, 2.4 ka (Table 6, framed values and Fig. 6B,C), in excellent agreement with those (at 11.1, 6.0, 4.4, 3.5, 2.7 and 2.4 ka) reported for the Vostok ice core (Yiou et al., 1994).

4. Discussion

4.1. D–O cycles and interhemispheric correlation

Millennial-scale oscillations have been recognized in several isotopic records of cores (RC11-83, TN57-21) located very close to, and at Site 1089 (Charles et al., 1996; Ninnemann et al., 1999). These isotopic signatures are assumed to be proxies of events occurring both in the Northern ($\delta^{13}C$ of benthic foraminifera, tracing the strength of NADW production in the North Atlantic and its influence in the South Atlantic) and in the Southern Hemisphere ($\delta^{18}O$ of planktic foraminifera, a proxy for local temperature change). Since the synchronization of the time scales of Greenland and Antarctica ice cores is problematic (due to the variety of methods employed for their development and the relatively high gas age/ice age uncertainty for some of them), the presence of these records in the same core allows one to infer the phase relationship of temperature changes between the two hemispheres (Charles et al., 1996; Ninnemann et al., 1999). Based on these proxies, the climatic change in the Subantarctic South Atlantic has been demonstrated to be almost in phase with the δD (deuterium isotopic fractionation, a temperature proxy for Antarctica, expressed in ‰ deviation from Standard Mean Ocean Water) record at Vostok, and both these records lead the corresponding changes in Greenland by ca. 1.5 ka (Charles et al., 1996; Mortyn et al., submitted). However, all these isotopic records are overprinted by influences other than surface temperature and NADW production alone (Mackensen et al., 1993; Charles et al., 1996). These include seawater $\delta^{18}O$ changes, the ice-volume effect, meltwater pulses (for $\delta^{18}O$), changing intensity of surface-water productivity and organic flux to the seafloor (for $\delta^{13}C$). For this reason, our SSST record will be a less biased parameter for comparison with Vostok temperature changes and Greenland ice-core records, as it is not affected by any of the above-mentioned overprints.

The main characteristics of the Subantarctic/Subtropical records from the Southern Ocean seem to entail an early rapid cooling at the end of MIS 5e (5e/5d transition) and quasi-periodic oscillations of high frequency between MIS 5d and MIS 2, within a generally cold time period (Pichon et al., 1992). Both these characteristics are also displayed in our SSST estimates (Fig. 3A).

The paleotemperature evolution at ODP Site 1089 bears strong resemblance (Figs. 3A and 5F,G), both in general shape, timing and amplitude, to the $\delta^{18}O$ *Globigerina bulloides* record (Mortyn et al., submitted) available for the same core, and to the corresponding record for the Vostok ice core (Figs. 3D and 4B). The SSST oscillations observed in our record from 70 to 20 ka (D–O cycles) are, however, stronger (ca. 3–4°C) than the corresponding events recognized both at Vostok, in the isotopic record of Site 1089 (with the isotopic changes equivalent to ca. 2°C pulses), and in the Subantarctic Indian Ocean, where SSST changes by ca. 2–3°C (Pichon et al., 1992).

There is, moreover, a paleotemperature link between our sediment core and the Vostok ice core during the interval 40–20 ka (Fig. 3C,D), and the

timing of the interstadial peaks is in general agreement with similar events, phase-locked to temperature changes, occurring in the CH_4 record (Fig. 3B) of the GRIP ice core from Greenland (Chappellaz et al., 1993). The time relation between the GRIP CH_4 record and the paleotemperature records (Fig. 3B,C) is, however, uncertain, as the GRIP curve is plotted against a gas-age scale, which is several hundreds to 1000 yr younger than the ice-age scale for this time interval.

Nonetheless, the similarity in the general pattern of climatic variability during this time interval would indicate that climatic events are strongly locked between high southern and northern and Subtropical/Subantarctic latitudes during sudden warm events occurring within generally cold time intervals. The broad features of the Vostok air temperature and atmospheric greenhouse gases concentration records (Barnola et al., 1987; Chappellaz et al., 1990; Petit et al., 1999) are therefore of large geographical significance (Antarctica and part of the Southern Hemisphere).

The fact that we are able to recognize, in our SSST record, events which are roughly similar in timing and amplitude to the methane pulses in the GRIP ice core and their causally connected interstadial temperature peaks (the D–O cycles), demonstrates the global geographic extent of these events. The stronger expression of these sudden warming events in our record compared to Vostok may be explained by the stronger influence of oceanographic (migrations of the STF) and atmospheric (changes in the water vapor and greenhouse gases content of air, with associated feedback mechanism over climate) processes at Subtropical/Subantarctic compared to polar southern latitudes. In particular, Site 1089 was probably close to the STF between 70 and 20 ka, and sudden changes in the position and/or strength of this front could have caused the high-frequency climatic instability observed during this time interval (Fig. 3). The front position would in turn be influenced by changes in wind stress fields and strength of the westerlies, which are reported to have a major role in controlling SSST gradients in the Southern Ocean (White and Peterson, 1996; Ninnemann et al., 1999).

Another indication of millennial-scale variability and interhemispheric interplay is the presence of episodes of ice-rafted debris (IRD) deposition between 20 and 74 ka in the Southern Ocean (Kanfoush et al., 2000). These episodes have also been recognized at a Subantarctic location (Core TTN057-21, 41°S), close to Core 1089 position, and are accompanied by increases in $\delta^{13}C$ of benthic foraminifera and $^{143}Nd/^{144}Nd$ ratios (Rutberg et al., 2000), both proxies for increased NADW production in the Nordic Seas. The IRD events seem to be correlated to some of the long-lasting D–O events recognized in the Greenland ice-core records. This would point to an antiphase correlation between the Northern and Southern Hemisphere, with IRD events in the South Atlantic associated with strong NADW production and warming in the North Atlantic.

4.2. Comparison of Terminations I and II structure

The glacial/interglacial SSST change at the last two terminations for Site 1089 is ca. 7°C (Figs. 3 and 4). This is in good agreement with other cores from the Subantarctic Zone: PS2082 (Brathauer and Abelmann, 1999) from the Atlantic Ocean, and RC11-120 (Hays et al., 1976) and MD84-527 (Pichon et al., 1992) from the Indian Ocean, all of which document SSST changes of 6–7°C for the last two terminations. Additional features recognizable in our SSST record include the sudden cooling events present at both terminations, and the higher climatic variability during MIS 5 (with several sudden cooling transitions of 3–4°C prior to 70 ka). A comparison of the detailed SSST evolution of our core across the last two terminations to the corresponding Vostok temperature changes (Fig. 4) follows:

At Termination II, SSST starts to increase by a few degrees in our core at ca. 139 ka (Fig. 4D), in parallel to the temperature increase at Vostok. At 132 ka, however, a ca. 3°C cooling occurs at our location, not matched in the Vostok temperature record. The major transition follows, with a warming of 5.5°C occurring within less than 1 kyr. A second 3°C cooling takes place at ca. 130–131 ka, after which temperatures rise again and reach maximum values (19°C) at 128 ka, also

when the Vostok temperature reaches its maximum.

We name the first cooling 'ACR-II event' and the second cooling 'YD-II event'. Their names refer to the similar variability displayed by these events compared to the ACR and YD events recognized at Termination I (and defined in ice cores from Byrd Station and Greenland, respectively), but have no causal implication. This implies that the ACR-II and YD-II might have been caused by processes and mechanisms different to those responsible for the ACR and YD. The presence of both events in our core could derive from its position in a 'boundary area', where the influence of processes occurring in both hemispheres can be recorded. In this respect, the first event could be caused by Southern Hemisphere ice-sheet breakdown and release of sea ice from the Rønne ice shelf, becoming unstable due to sea-level rise and/or a slight increase in temperature in the Southern Ocean. This event probably would have been relatively 'minor' and mostly connected to transient oceanic changes (and therefore not recorded in the 'continental' Vostok temperature record). The second cooling, however, could be a combined atmospheric/oceanic response to major ice-sheet collapses and disintegration (and associated changes in thermohaline circulation) occurring in the Northern Hemisphere, and caused by the sudden 5.5°C rise occurring in our record between 132 and 131 ka. The second cooling could, therefore, also have affected the Antarctic continent, and be represented by the short-lived plateau present in the Vostok temperature record just before the peak at 128 ka. The absence of this event in the planktic isotopic record (Fig. 5G) can be explained by the fact that the samples for which we estimated SSST are 'off-splice' in the 1089 core composite record, and isotopic measurements are not yet available for them.

At Termination I (Fig. 4C), SSST starts to increase at ca. 17–18 ka, roughly synchronously to Vostok. A 2°C cooling occurs between 12.3 and 14 ka, correlating to the slowdown in temperature rise evident at Vostok. The major warming starts at ca. 12 ka, with a SSST increase of ca. 5°C in less than 1 kyr, and it is followed by a short-lived 2°C cooling at ca. 11.3 ka. This sequence of events is exactly matched by the planktic isotope record (Fig. 3A), although the SSST changes lead the isotopic shifts by a few kyr.

Similarly to Termination II, we name the first cooling 'ACR-I event' and the second cooling 'YD-I event'. Once again, it is stressed that these names have no causal or, in this case (Termination I), chronological implication, as they cannot be directly compared to the 'real' ACR and YD events due to the different chronologies of the records.

However, ACR-I seems to occur almost synchronously to the ACR recognized at Vostok (Fig. 4C,D) and in the $\delta^{18}O$ planktic record of Core RC11-83 (Charles et al., 1996), and therefore, according to the latter authors, would probably lead the YD recognized in the GRIP ice core by at least 1 ka.

Investigation of the Vostok ice-core paleotemperature record led Petit et al. (1999) to state that, unlike Termination I, there is no clear temperature anomaly equivalent to the ACR during older terminations (however, they admitted that their sample resolution might not have been adequate to spot such an event). Other authors have indicated the possibility of a sudden cooling event during Termination II, at least in areas close to the North Atlantic (Haake and Pflaumann, 1989; Sarnthein and Tiedemann, 1990; Seidenkrantz et al., 1995).

However, cooling events (ACR-I, ACR-II and YD-I, YD-II) are present in our SSST record (Fig. 4) at Termination I and at Termination II, and could imply that, given a sufficient time resolution and appropriate geographic location, these events are recognizable even in marine records, and could be related to a common mechanism of change between full glacial and interglacial conditions.

In our core, the magnitude of the temperature increase (ca. 7°C), the time span over which it occurs (10–12 ka), as well as the presence in between of short-lived cooling events with a drop in temperature of several degrees, all point towards a similarity between the last two terminations (see also end of 3.1. Paleotemperatures).

The sequence of events connected to terminations (Petit et al., 1999) could therefore be the same, but its expression could be influenced by

the geographic location of the study area itself, and its sensitivity in recording the different climatic proxies connected to those events.

Another interesting characteristic of our paleotemperature record is the slightly colder (ca. 1°C) maximum glacial conditions during MIS 2 compared to MIS 6, right before the last two terminations. While this is not typical for either ice-core or oceanic records from higher latitudes, it can also be observed in oceanic alkenone-based paleotemperature records from intertropical (equatorial) latitudes of the South Atlantic (Schneider et al., 1995). According to their results, MIS 6 is warmer at this site than MIS 2, and the associated $\delta^{18}O$ isotopic changes in planktic foraminifera are not consistent with the observed temperature difference, being similar between the two isotopic stages in some cores, and being lighter in MIS 2 than in MIS 6 in some other cores (e.g. at 20°S, close to the Walvis Ridge).

This discrepancy between isotopic and paleotemperature records at the last two terminations is confirmed in our record, with similar SSST changes (Fig. 3A) at both terminations (ca. 7°C) associated with different $\delta^{18}O$ isotopic changes in planktic foraminifera: 1.5 and 2.5‰ at Terminations I and II, respectively (Mortyn et al., submitted). This difference between the last two terminations could be partly due to different amounts of polar ice volume, sea-level rises, and meltwater pulses, which would radically distort the paleo-SSST interpretation of the planktic isotopic record (Sarnthein and Tiedemann, 1990). In particular, MIS 2 could have been characterized by more extensive polar ice caps and/or more widespread meltwater injections at Subantarctic latitudes compared to MIS 6. Both these effects would have as a result the dampening of the paleotemperature signal as derived from $\delta^{18}O$ isotopic changes in comparison to independent SSST estimations.

Studies spanning a longer time period than one single termination (Sarnthein and Tiedemann, 1990; Pichon et al., 1992) provide important indications for differences and similarities between different terminations. Even within a single termination, however, the climatic response can be complex and depend on the geographic location. As an example of this, SSST estimates based on a diatom-transfer function for a Subantarctic (43°S) and an Antarctic (55°S) core in the Indian sector of the Southern Ocean (Pichon et al., 1992) indicate that the climatic evolution of the former core during the last climatic cycle closely matches available paleotemperature records from Subtropical latitudes, such as Core RC11-120 (Martinson et al., 1987), while the latter core seems to be coupled to the climatic evolution documented in the Vostok ice core.

The direct comparison of planktic isotopic records from Site 1089 (Mortyn et al., submitted) with our results for radiolarian-based SSST from the same sample interval shows that SSST changes at Termination II (Figs. 3A and 5F,G) lead $\delta^{18}O$ planktic (*Globigerina bulloides*) isotopic changes, which in turn lead $\delta^{18}O$ isotopic changes in the benthic foraminifer *Cibicidoides* spp. (Charles et al., 1996; Mortyn et al., submitted). This pattern would therefore confirm the observation that, in the Southern Ocean, climate changes in surface waters (such as SSST estimates) respond quickly to orbital forcings. The surface isotopic signal (not exclusively influenced by surface-water temperatures) lags behind by 1–2 ka, and the deep-water isotopic signal (mainly a global signal, caused by continental ice-volume changes, but also imprinted by local changes in deep-water temperatures) occurs 4–5 ka later than sea-surface temperature changes (Pichon et al., 1992; Charles et al., 1996; Labeyrie et al., 1996; Brathauer and Abelmann, 1999). The same sequence of events seems to hold true for Termination I, at least for SSST and planktic $\delta^{18}O$ changes; for this time period, benthic $\delta^{18}O$ results are not available for Site 1089.

This relative timing of the deglaciation, and its expression in different areas of the world, is of particular interest when trying to identify the mechanism responsible for worldwide transmission of climatic changes. In fact, changes in the thermohaline circulation have been invoked as a possible means for interhemispheric climate connection. This classic 'conveyor belt' hypothesis has, however, been questioned recently, as climate reacts in a more complex way (particularly at millennial time scales) than with a direct response to

changes occurring in the North Atlantic and surrounding areas, and then spreading worldwide from there (Charles et al., 1996; Ninnemann et al., 1999).

According to the classic view, a reduction of NADW formation in the Nordic Seas (caused by meltwater discharges in the North Atlantic) would have as a consequence both a cooling of the North Atlantic and surrounding areas (reduced input of warmer surface waters from the south) and a resulting warming of most of the equatorial Atlantic and Southern Ocean (Crowley, 1992; Schiller et al., 1997).

Therefore, this hypothesis (i.e. the changes are transferred by the ocean) would gain support if the climatic response of the two hemispheres were in 'antiphase', while an 'in phase' relationship (linked to a globally synchronous atmospheric transfer mechanism) would argue against it.

The 'antiphase' relationship between the two hemispheres is confirmed by some studies:

– modelling experiments showing a Southern Ocean warming in correspondence to NADW reduction and cooling in the North Atlantic (Crowley, 1992; Schiller et al., 1997);

– the comparison between the Byrd (Antarctica) and the GRIP (Greenland) ice cores, with the ACR in phase with the Bølling–Allerød warm period in Greenland, and an Antarctic warming step corresponding to the YD cold event (Jouzel et al., 1995; Sowers and Bender, 1995); and

– alkenone SSST estimates from the equatorial (10°N) western Atlantic (Rühlemann et al., 1999), with high SSST during the Heinrich event H1 and the YD, and low SSST during the Bølling–Allerød chronozones.

However, an 'in phase' relationship of climatic change between both hemispheres is suggested by other datasets:

– the Taylor Dome (Antarctica) ice core (Steig et al., 1998);

– high altitude temperatures from Bolivia (Thompson et al., 1998);

– glacier advance records in the Andean mountains (Lowell et al., 1995);

– warming events synchronous to the D–O cycles of GRIP recognized at 20°S in the Indian Ocean (Bard et al., 1997); and

– cooling events, synchronous to YD and H1, in alkenone-based SSST in the eastern Atlantic (Zhao et al., 1995).

Another complicating factor is that the time relation between cooling events occurring at terminations (such as the YD) and Heinrich events (indicators of meltwater discharges and circulation changes in the North Atlantic) seems not to hold true for the YD itself (Sarnthein and Tiedemann, 1990). The latter authors demonstrated, in a sediment core off NW Africa, that there are no indications of causal relationships between the YD, as observed in the $\delta^{18}O$ benthic record, and the associated $\delta^{13}C$ benthic record, since the $\delta^{13}C$ event (supposed to represent changes in the intensity of NADW production) occurs later than the YD. The interpretation of the $\delta^{13}C$ record as a pure NADW production proxy is, however, problematic off NW Africa, as it is influenced by variations in the strength of the Cape Blanc upwelling system, with changes in surface-water productivity that would strongly distort both the $\delta^{13}C$ and the planktic $\delta^{18}O$ signals (e.g. no YD event is recognizable in the latter).

Nonetheless, this demonstrates that different climatic 'events' (YD, ACR, D–O cycles, cooling events during interglacials) are most likely triggered and/or amplified by different mechanisms and feedbacks, which, for the same kind of event, might even change according to the geographic location of the record documenting the event.

The geographic extent of the YD-type of event is therefore relevant: while it has been recognized as far from the North Atlantic as in the planktic $\delta^{18}O$ record of the Sulu Sea, tropical western Pacific (Linsley and Thunell, 1990), ice cores from Bolivia (Thompson et al., 1998), and other continental records from South America (Markgraf, 1993), a study of climate proxies in lacustrine deposits from South Georgia Island (54°S) demonstrated climatic stability during the YD chronozone at this location (Rosqvist et al., 1999).

Since the climatic patterns observed during the YD chronozone seem not to be restricted to the high latitudes of the North Atlantic, their expression and timing in the different parts of the world could be connected to causes (local changes in salinity and/or hydrology) other than exclusively

meltwater pulses and circulation changes occurring in the North Atlantic.

The influence of Northern Hemisphere forcing mechanisms (through NADW variability, as expressed in Southern Ocean proxy records) on climatic changes in the Southern Hemisphere therefore remains highly controversial. Climatic changes seem to be connected to NADW variability, but not caused by it, since the Northern Hemisphere climate signal lags that of the Southern Hemisphere by ca. 1500 yr (Charles et al., 1996). This lead of the Southern Ocean sea-surface climatic change with respect to the Northern Hemisphere ice-volume changes has also been observed by other authors in both the Atlantic (Brathauer and Abelmann, 1999) and Indian sectors of the Southern Ocean (Pichon et al., 1992; Labeyrie et al., 1996).

However, the final word in this controversy of the relative timing of climatic changes (and the mechanisms causing them) between the Northern and Southern Hemisphere has not yet been delivered. This mainly derives from the difficulty in accurately interpreting, dating, and correlating multiple proxies from widely different climatic archives (ice and sediment cores, terrestrial deposits). Each of these records deals with different assumptions and time uncertainties, which very often become so important as to make it impossible to establish cause and effect relationships between changes observed in the Northern and Southern Hemisphere. As an example of only one of these uncertainties, the dating of the MIS 5e/5d transition (at ca. 114 ka) in the stacked benthic $\delta^{18}O$ record (Martinson et al., 1987), widely used both for building age models for oceanic sediment cores, and as a key marker for developing some ice-core age models, has a standard error of ± 6 ka.

4.3. Climate variability and optima (MIS 1 and 5)

Sudden cooling events, similar to the three main events recognized in the Nordic Seas at 127–126, 122–121 and ca. 117 ka (Fronval and Jansen, 1996, 1997), are the main feature of our Eemian paleotemperature record (Fig. 3A), and occur at 124, 118.5 and 114 ka, i.e. apparently 3 kyr later than in the Nordic Seas. This difference in timing is, however, still within the error uncertainty of age models based on the SPECMAP stack (Martinson et al., 1987: table 2), and it cannot be ruled out that these events might even be synchronous.

The second event (at ca. 118.5 ka) could be the same cooling event recognized in the Southern Ocean using different climatic proxies, i.e. diatom- (Pichon et al., 1992) and alkenone-based SSST estimates (Ikehara et al., 1997), and $\delta^{13}C$ of benthic foraminifera (Ninnemann et al., 1999).

The climatic variability of MIS 5 has been confirmed, for Site 1089, by $\delta^{18}O$ of planktic foraminifera (Ninnemann et al., 1999). These authors suggest that the millennial-scale excursions in $\delta^{18}O$ during stages 5a, 5b and 5e are equivalent, or even greater, than those observed during MIS 2–4, with less intense fluctuations in the interval 95–115 ka.

This variability appears even more strongly in our SSST record (Fig. 3A), since prominent interglacial cooling events within MIS 5 are also present at 104 and 97 ka (during substage 5c), and at 78 ka (in the middle of substage 5a). In particular, the cooling at 104 ka could be correlative to the Montaigue event recognized in the continental pollen record of la Grand Pile in France (Woillard, 1978; Kukla et al., 1997), and also recognized in a core from the Bahama Outer Ridge (Keigwin and Jones, 1994) whose climatic evolution during substage 5c is very similar to that in our core.

The interval 95–115 ka is no exception, as SSST displays strong changes compared to the more subdued *Globigerina bulloides* $\delta^{18}O$ signal (Fig. 3A). Even if the observed isotopic changes were exclusively attributed to SSST changes, their maximum magnitude during this time interval (ca. 0.7‰) would represent only 3.2°C temperature differences, while our estimations indicate SSST shifts of up to 4.5°C during the same time interval.

The same pattern of lower variability of the planktic foraminifer *N. pachyderma* $\delta^{18}O$ record compared to diatom-based SSST estimates has been observed, during MIS 5, in other cores from Subantarctic latitudes in the Indian sector

of the Southern Ocean (Pichon et al., 1992). The latter authors interpreted this difference as caused by local variability in surface temperature and salinity, and sensitivity to isotopically light meltwater peaks, but could also be caused by changes in the living depth of *N. pachyderma* in cold and warm time intervals.

Our SSST estimates also display evidence of climatic deterioration for the current interglacial (MIS 1). In fact, relatively cooler temperatures seem to occur at ca. 9 ka (Fig. 4C) and could be equivalent to the 8.2-ka cooling event of the North Atlantic and Greenland (Alley et al., 1997; Mayewski et al., 1997; von Grafenstein et al., 1998).

The presence of these cooling events within the last two interglacial intervals indicates that the climate system can experience rapid changes not only during cold, glacial time periods but also during warm, interglacial time periods.

The recognition of these cooling events in our sedimentary record from the Southern Ocean, during both last two climatic 'optima' of the last glacial cycle, witnesses their importance as global, or at least hemispheric, events. They are therefore not strictly limited to polar ice cores and/or areas surrounding the North Atlantic, and question the general applicability of the 'conveyor belt' hypothesis to all areas of the world ocean. In fact, while these events could still be caused by a shutdown or reduction of NADW production (due to iceberg and meltwater discharges from the Laurentide and Fennoscandian ice sheets) in areas close to the North Atlantic, their occurrence in Southern Ocean latitudes seems to be connected instead to reorganizations of surface and/or deep-ocean circulation, meltwater peaks of local importance, or even atmospheric processes (e.g. intensified precipitations). Their occurrence during climatic optima such as MIS 1 and 5 would moreover complicate their explanation in connection to iceberg and major meltwater discharges, since the warmer temperatures during these time periods would drastically reduce both the extent of the ice sheets at both poles, and the northernmost reaches of icebergs, which would melt before even reaching Subantarctic/Subtropical latitudes.

These arguments could point towards a different mechanism causing these events, possibly an atmospheric mechanism (since the events seem to be almost synchronous between the Northern and the Southern Hemisphere), such as a change in the hydrological cycle at Subtropical/Subantarctic latitudes, implying stronger precipitation and/or less evaporation regimes causing a cooling climatic effect similar to, but genetically different from, a meltwater event.

4.4. Spectral analysis, high-frequency non-linear climatic responses to orbital forcing, and internal mechanisms

The orbital forcing of climatic change has long been recognized in oceanic records (Hays et al., 1976), however, there are indications of possible non-linear responses of the climatic system to orbital forcing, including rapid events of almost full glacial to interglacial extent and very short duration, which we identified in our record, particularly during MIS 3 and 4 (Fig. 3A).

Non-linear responses of climatic change to external forcing mechanisms (through positive feedbacks amplifying the 'forced' climatic change) clearly play a fundamental role at glacial to interglacial transitions. In fact, the renowned increase in greenhouse gases (CO_2, CH_4, water vapor) at these transitions is only able to explain temperature increases of a few °C (the 'direct forcing'), with the rest of the temperature increase, actually the most conspicuous portion of it, being accounted for by feedback mechanisms (the 'non-linear' response).

MTM and evolutive spectrum analysis have been applied to the Vostok paleotemperature record (Yiou et al., 1991), and both orbital and additional stable peaks (at 11.1, 6.0, 4.4, 3.5, 2.7 and 2.4 kyr) have been recognized and attributed to harmonics and combination tones of the orbital frequencies, indicating that non-linear responses to orbital forcings indeed play an important role in paleoclimatic variability.

A direct comparison of our results (Fig. 6, Table 6) to those reported for the Vostok ice core is possible since the two cores roughly span the same time interval (ca. 160 ka) and the average

sample resolution is of the same order (0.6 kyr on average for our core, 0.1 kyr for Vostok).

All the high-frequency spectral peaks recognized in the Vostok temperature record are very close to the periodicities recognized in our record (Table 6, framed values) and, more importantly, are combination tones of orbital periods: the two precessional and the obliquity cycles, see Yiou et al. (1991: table 3). They would therefore all be connected to the operation of non-linear mechanisms, such as ice-albedo and precipitation-temperature feedbacks or changes in atmospheric chemical composition.

Spectral analysis has also been applied to percent $CaCO_3$ time series from the Bermuda Rise, in the western Subtropical North Atlantic (Keigwin and Jones, 1994), resulting in two significant peaks (at the 80% confidence level) at 3.6 and 4.5 ka. These peaks are interpreted as being connected to the variability observed in the MIS 3 portion of the core, with a series of events correlating to the D–O cycles of Greenland ice cores. These periods are also evident in our Subantarctic SSST spectrum (Table 6: 3.6 and 4.2 ka), demonstrating a close agreement between these periodicities in other widely separated areas of the globe, such as the Antarctic ice cap (Yiou et al., 1991: 3.5 and 4.4 ka) and the Subtropical North Atlantic (Keigwin and Jones, 1994: 3.6 and 4.5 ka).

The correspondence of spectral peaks would therefore confirm the close link between climatic change occurring at Subantarctic/Subtropical latitudes and the climatic history of Vostok and of polar ice cores in general. The climatic linkage mechanism could be the Subtropical/Subantarctic location of moisture sources for the precipitation falling at Vostok and recorded in the corresponding δD records. This would be particularly true for MIS 3, when sudden warming events occur within a glacial time period.

Uncertainties in the location of the spectral peaks connected to age-scale errors can be ruled out for the high frequencies, as high-frequency peaks (1/10 to 1/4 cycles/kyr) are stable in position and are not affected strongly by time-scale errors (Yiou et al., 1994).

Periods not connected to orbital periodicities and sum tones would instead represent purely internal mechanisms, which can be deterministic, quasi-periodic components of the signal, such as changes in the ocean–atmosphere–land monsoon system for cores located in the tropical belt (Kutzbach, 1981), periods of ca. 7–8 kyr in Indian Ocean cores; or changes in thermohaline circulation (Welander, 1986), periods of 11.2 kyr in the North Atlantic. These periods are quite close to those of two significant peaks we recognized in our record (Table 6, periods of 7.7 and 10.9 kyr), with the latter probably being a precession harmonic instead, and therefore falling in the previous non-linear mechanisms.

Three different classes of phenomena therefore have a direct influx on the climatic evolution of our record, as has been demonstrated previously for the Vostok ice core (Yiou et al., 1991):

– orbital (external) forcings, mostly related to the precession cycle (periods of 29.2, 23.3 ka in our SSST record);

– non-linear responses to orbital forcings, such as ice-albedo changes, variations in atmospheric composition and other feedbacks (periods of 10.9, 6.1, 4.2, 3.6, 2.8, 2.4 ka); and

– internal (quasi-periodic) mechanisms, probably related to changes in the thermohaline circulation strength (period of 7.7 ka).

5. Conclusions

– Radiolarian-based paleotemperature estimations allowed us to reconstruct the detailed paleotemperature history of the last 160 ka, recovered from ODP Site 1089 and Core PS2821, located at the present position of the South Atlantic STF. A 7°C warming occurs at Termination II, with maximum interglacial temperatures occurring in the earlier part of substage 5e and being ca. 3°C warmer than present temperature at the core location.

– The SSST changes occur earlier than the corresponding shift in $\delta^{18}O$ values for both planktic and benthic foraminifera from the same core (Mortyn et al., submitted), indicating a lead of Southern Ocean SSST compared to global ice-volume changes.

– High-frequency, millennial-scale climatic variability has been documented for MIS 3 and part of MIS 4, with sudden temperature variations of almost the same magnitude as those observed at the transitions between glacial and interglacial times. These changes are probably associated with rapid oceanic/atmospheric perturbations and reorganizations (possibly affecting the STF position and/or the salinity and temperature gradients across it) and seem to be the Southern Ocean equivalent to the D–O cycles recognized in the $\delta^{18}O_{ice}$ record of the GRIP and GISP ice cores from Greenland.

– Sudden cooling events, similar to the YD cold spell of the North Atlantic and to the ACR event documented in some Antarctic ice cores, have been recorded for both Terminations I and II. The presence of these cold spells (ACR-I, ACR-II and YD-I, YD-II events) suggests a common mechanism of change between full glacial and interglacial conditions, at least for the last two terminations.

– The climatic optima in the Southern Ocean sedimentary record (MIS 1 and 5e) display evidence of climatic variability, as sudden cooling events are recognized in our record at 124, 118.5, 114 ka (MIS 5) and 9 ka (MIS 1). Other cooling events occur in our record during warm time intervals, e.g. at 104 and 97 ka (during substage 5c), and at 78 ka (in the middle of substage 5a). The 118.5-ka event could be the same as recognized in other areas of the Southern Ocean (Pichon et al., 1992; Ikehara et al., 1997; Ninnemann et al., 1999), while the 9-ka event could be equivalent to the 8.2-ka cooling event of the North Atlantic (Alley et al., 1997; Mayewski et al., 1997; von Grafenstein et al., 1998). The recognition of these events in our sedimentary record from the Southern Ocean witnesses their importance as global, or at least hemispheric, events not strictly limited to polar ice cores and/or areas surrounding the North Atlantic.

– Spectral analysis of the temperature record from our cores is in excellent agreement with similar results obtained from the Vostok ice-core temperature record and stresses the importance of both orbital (particularly precession-related) forcing, the non-linear response of the climatic system to this precessional forcing (feedbacks), and some other internal mechanism (changes in the thermohaline circulation strength?).

– The correspondence of spectral peaks (periods of 3.6 and 4.2 ka) with other records from Subtropical latitudes in the North Atlantic (3.6 and 4.5 ka, see Keigwin and Jones, 1994), and from the Antarctic ice cap (3.5 and 4.4 ka, see Yiou et al., 1991) confirms the close link between climatic change occurring at Subantarctic/Subtropical latitudes and the climatic history of polar ice cores.

Acknowledgements

Core repository facilities (Geology Institute, Bremen University for ODP and R/V '*Meteor*' cores and AWI, Bremerhaven for R/V '*Polarstern*' cores) are gratefully acknowledged. Rainer Gersonde provided interesting discussions and feedback throughout this study. We also would like to thank the suggestions and comments of the final reviewers: Kjell Bjørklund and Nicklas Pisias. Correlations between cores have been performed using the AnalySeries software (Paillard et al., 1996). The CABFAC, THREAD and REGRESS routines of the IKM for Q-mode factor analysis have been run using the PaleoToolBox and MacTransfer software packages (Sieger et al., 1999). Some of the oceanographic data have been extracted using the program Ocean Data View (Schlitzer, 2000). We thank Ute Bock, Ruth Cordelair and Inge Klappstein for providing laboratory assistance. This research was supported by the Deutsche Forschungsgemeinschaft through Sonderforschungsbereich (SFB) 261. This is SFB contribution 326.

References

Abelmann, A., 1992. Radiolarian flux in Antarctic waters (Drake Passage, Powell Basin, Bransfield Strait). Polar Biol. 12, 357–372.

Abelmann, A., Gersonde, R., 1991. Biosiliceous particle flux in the Southern Ocean. Mar. Chem. 35, 503–536.

Abelmann, A., Brathauer, U., Gersonde, R., Sieger, R., Zielinski, U., 1999. Radiolarian-based transfer function for the

estimation of sea surface temperatures in the Southern Ocean (Atlantic sector). Paleoceanography 14, 410–421.

Adkins, J.F., Boyle, E.A., Keigwin, L., Cortijo, E., 1997. Variability of the North Atlantic thermohaline circulation during the last interglacial period. Nature 390, 154–156.

Alley, R.B., Mayewski, P.A., Sowers, T., Stuiver, M., Taylor, K.C., Clark, P.U., 1997. Holocene climatic instability: A prominent widespread event 8200 yr ago. Geology 25, 483–486.

Bard, E., Rostek, F., Sonzogni, C., 1997. Interhemispheric synchrony of the last deglaciation inferred from alkenone palaeothermometry. Nature 385, 707–710.

Barnola, J., Raynaud, D., Korotkevich, Y.S., Lorius, C., 1987. Vostok ice core provides 160,000-year record of atmospheric CO_2. Nature 329, 408–414.

Blunier, T., Schwander, J., Stauffer, B., Stocker, T., Dällenbach, A., Indermühle, A., Tschumi, J., Chappellaz, J., Raynaud, D., Barnola, J.M., 1997. Timing of the Antarctic Cold Reversal and the atmospheric CO_2 increase with respect to the Younger Dryas event. Geophys. Res. Lett. 24, 2683–2686.

Blunier, T., Chappellaz, J., Schwander, J., Dällenbach, A., Stauffer, B., Stocker, T.F., Raynaud, D., Jouzel, J., Clausen, H.B., Hammer, C.U., Johnsen, S.J., 1998. Asynchrony of Antarctic and Greenland climate change during the last glacial period. Nature 394, 739–743.

Bond, G., Broecker, W.S., Johnsen, S.J., McManus, J., Labeyrie, L.D., Jouzel, J., Bonani, G., 1993. Correlations between climate records from North Atlantic sediments and Greenland ice. Nature 365, 143–147.

Brathauer, U., Abelmann, A., 1999. Late Quaternary variations in sea surface temperatures and their relationships to orbital forcing recorded in the Southern Ocean (Atlantic sector). Paleoceanography 14, 135–148.

Chappellaz, J., Barnola, J.M., Raynaud, D., Korotkevich, Y.S., Lorius, C., 1990. Ice-core record of atmospheric methane over the past 160,000 years. Nature 345, 127–131.

Chappellaz, J., Blunier, T., Raynaud, D., Barnola, J.M., Schwander, J., Stauffer, B., 1993. Synchronous changes in atmospheric CH_4 and Greenland climate between 40 and 8 kyr BP. Nature 366, 443–445.

Charles, C.D., Lynch-Stieglitz, J., Ninnemann, U.S., Fairbanks, R.G., 1996. Climate connections between the hemisphere revealed by deep sea sediment core/ice core correlations. Earth Planet. Sci. Lett. 142, 19–27.

Cortijo, E., Duplessy, J.C., Labeyrie, L., Leclaire, H., Duprat, J., vanWeering, T.C.E., 1994. Eemian cooling in the Norwegian Sea and North Atlantic ocean preceding continental ice-sheet growth. Nature 372, 446–449.

Cortijo, E., Yiou, P., Labeyrie, L., Cremer, M., 1995. Sedimentary record of rapid climatic variability in the North Atlantic Ocean during the last glacial cycle. Paleoceanography 10, 911–926.

Crowley, T.J., 1992. North Atlantic Deep Water cools the southern hemisphere. Paleoceanography 7, 489–498.

Dansgaard, W., Johnsen, S.J., Clausen, H.B., Dahl-Jensen, D., Gundestrup, N.S., Hammer, C.U., Hvidberg, C.S., Steffensen, J.P., Sveinbjörnsdottir, A.E., Jouzel, J., Bond, G., 1993. Evidence for general instability of past climate from a 250-kyr ice-core record. Nature 364, 218–220.

Field, M.H., Huntley, B., Müller, H., 1994. Eemian climate fluctuations observed in a European pollen record. Nature 371, 779–783.

Fronval, T., Jansen, E., 1996. Rapid changes in ocean circulation and heat flux in the Nordic seas during the last interglacial period. Nature 383, 806–810.

Fronval, T., Jansen, E., 1997. Eemian and early Weichselian (140–60 ka) paleoceanography and paleoclimate in the Nordic seas with comparisons to Holocene conditions. Paleoceanography 12, 443–462.

Grootes, P.M., Stuiver, M., White, J.W.C., Johnsen, S., Jouzel, J., 1993. Comparison of oxygen isotope records from the GISP2 and GRIP Greenland ice cores. Nature 366, 552–554.

Haake, F.W., Pflaumann, U., 1989. Late Pleistocene foraminiferal stratigraphy on the Vøring Plateau, Norwegian Sea. Boreas 18, 343–356.

Hays, J.D., Imbrie, J., Shackleton, N.J., 1976. Variations in the Earth's orbit: Pacemaker of the Ice Ages. Science 194, 1121–1132.

Ikehara, M., Kawamura, K., Ohkouchi, N., Kimoto, K., Murayama, M., Nakamura, T., Oba, T., Taira, A., 1997. Alkenone sea surface temperature in the Southern Ocean for the last two deglaciations. Geophys. Res. Lett. 24, 679–682.

Johnsen, S.J., Clausen, H.B., Dansgaard, W., Fuhrer, K., Gunderstrup, N.S., Hammer, C.U., Iverssen, P., Jouzel, J., Stauffer, B., Steffensen, J.P., 1992. Irregular glacial interstadials recorded in a new Greenland ice core. Nature 359, 311–313.

Jouzel, J., Vaikmae, R., Petit, J.R., Martin, M., Duclos, Y., Stievenard, M., Lorius, C., Toots, M., Mélières, M.A., Burkle, L.H., Barkov, N.I., Kotlyakov, V.M., 1995. The two-step shape and timing of the last deglaciation in Antarctica. Clim. Dyn. 11, 151–161.

Kanfoush, S.L., Hodell, D.A., Charles, C.D., Guilderson, T.P., Mortyn, P.G., Ninnemann, U.S., 2000. Millennial-scale instability of the Antarctic ice sheet during the last glaciation. Science 288, 1815–1818.

Keigwin, L.D., Jones, G.A., 1994. Western North Atlantic evidence for millennial-scale changes in ocean circulation and climate. J. Geophys. Res. 99, 12397–12410.

Kukla, G., McManus, J.F., Rousseau, D.D., Chuine, I., 1997. How long and how stable was the last interglacial? Quat. Sci. Rev. 16, 605–612.

Kutzbach, J.E., 1981. Monsoon climate of the early Holocene: Climate experiment with the Earth's orbital parameters for 9000 years ago. Science 214, 59–61.

Labeyrie, L., Labracherie, M., Gorfti, N., Pichon, J.J., Vautravers, M., Arnold, M., Duplessy, J.C., Paterne, M., Michel, W., Duprat, J., Caralp, M., Turon, J.L., 1996. Hydrographic changes of the Southern Ocean (southeast Indian sector) over the last 230 kyr. Paleoceanography 11, 57–76.

Levitus, S., Boyer, T., 1994. World Ocean Atlas 1994, Vol. 4: Temperature. NOAA Atlas NESDIS 4, Washington, DC, 117 pp.

Linsley, B.K., Thunell, R.C., 1990. The record of deglaciation in the Sulu Sea: Evidence for the Younger Dryas event in the tropical western Pacific. Paleoceanography 5, 1025–1039.

Lototskaya, A., Ganssen, G.M., 1999. The structure of Termination II (penultimate deglaciation and Eemian) in the North Atlantic. Quat. Sci. Rev. 18, 1641–1654.

Lowell, T.V., Heusser, C.J., Andersen, B.G., Moreno, P.I., Hauser, A., Heusser, L.E., Schlüchter, C., Marchant, D.R., Denton, G.H., 1995. Interhemispheric correlation of Late Pleistocene glacial events. Science 269, 1541–1549.

Mackensen, A., Hubberten, H.W., Bickert, T., Fisher, G., Fütterer, D.K., 1993. The $\delta^{13}C$ in benthic foraminiferal test of *Fontbotia wuellerstorfi* (Schwager) relative to the $\delta^{13}C$ of dissolved inorganic carbon in Southern Ocean deep water: Implications for glacial ocean circulation models. Paleoceanography 8, 587–610.

Markgraf, V., 1993. Younger Dryas in southernmost South America: An update. Quat. Sci. Rev. 12, 351–355.

Martinson, D.G., Pisias, N.G., Hays, J.D., Imbrie, J., Moore, T.C., Shackleton, N.J., 1987. Age dating and the orbital theory of the Ice Ages: Development of a high-resolution 0 to 300,000-year chronostratigraphy. Quat. Res. 27, 1–29.

Maslin, M.A., Tzedakis, C., 1996. Sultry last interglacial gets sudden chill. EOS (Trans. Am. Geophys. Union) 77, 353–354.

Maslin, M.A., Sarnthein, M., Knaack, J.J., Grootes, P., Tzedakis, C., 1998. Intra-interglacial cold events: An Eemian–Holocene comparison. In: Cramp, A., MacLeod, C., Lee, S.V., Jones, E.J. (Eds.), Geological Evolution of the Ocean Basin: Results from the Ocean Drilling Program 131. Geological Society London, Spec. Publ., pp. 91–99.

Mayewski, P.A., Meeker, L.D., Twickler, M.S., Whitlow, S., Yang, Q., Lyons, W.B., Prentice, M., 1997. Major features and forcing of high-latitude Northern Hemisphere atmospheric circulation using a 110,000-year-long glaciochemical series. J. Geophys. Res. 102, 26345–26365.

McManus, J.F., Bond, G.C., Broecker, W.S., Johnsen, S., Labeyrie, L., Higgins, S., 1994. High-resolution climate records from the North Atlantic during the last interglacial. Nature 371, 326–329.

Mortyn, P.G., Charles, C.D., Hodell, D.A., Ninnemann, U.S., submitted. Building marine sediment analogs to the Vostok ice core. J. Geophys. Res.

Naval Oceanography Command Detachment, 1985. Sea Ice Climatic Atlas, Vol. 1, Antarctic. National Space Technology Laboratory, Asheville, NC, 131 pp.

Ninnemann, U.S., Charles, C.D., Hodell, D.A., 1999. Origin of global millennial scale climate events: Constraints from the Southern Ocean deep sea sedimentary record. In: Clark, P.U., Webb, R.S., Keigwin, L.D. (Eds.), Mechanisms of Global Climate Change. American Geophysical Union, Washington, DC, pp. 99–112.

Olbers, D., Gouretski, V., Seiß, G., Schröter, J., 1992. Hydrographic Atlas of the Southern Ocean. Alfred Wegener Institute for Polar and Marine Research, Bremerhaven.

Paillard, D., Labeyrie, L., Yiou, P., 1996. Macintosh program performs time-series analysis. EOS (Trans. Am. Geophys. Union) 77, 379.

Peterson, R.G., Stramma, L., 1991. Upper-level circulation in the South Atlantic Ocean. Prog. Oceanogr. 26, 1–73.

Petit, J.R., Jouzel, J., Raynaud, D., Barkov, N.I., Barnola, J.M., Basile, I., Bender, M., Chappellaz, J., Davis, M., Delaygue, G., Delmotte, M., Kotlyakov, V.M., Legrand, M., Lipenkov, V.Y., Lorius, C., Pépin, L., Ritz, C., Saltzman, E., Stievenard, M., 1999. Climate and atmospheric history of the past 420,000 years from the Vostok ice core, Antarctica. Nature 399, 429–436.

Pichon, J.J., Labeyrie, L.D., Bareille, G., Labracherie, M., Duprat, J., Jouzel, J., 1992. Surface water temperature changes in the high latitudes of the southern hemisphere over the last glacial–interglacial cycle. Paleoceanography 7, 289–318.

Rosqvist, G.C., Rietti-Shati, M., Shemesh, A., 1999. Late glacial to middle Holocene climatic record of lacustrine biogenic silica oxygen isotopes from a Southern Ocean island. Geology 27, 967–970.

Rühlemann, C., Mulitza, S., Müller, P.J., Wefer, G., Zahn, R., 1999. Warming of the tropical Atlantic Ocean and slowdown of thermohaline circulation during the last deglaciation. Nature 402, 511–514.

Rutberg, R.L., Hemming, S.R., Goldstein, S.L., 2000. Reduced North Atlantic Deep Water flux to the glacial Southern Ocean inferred from neodymium isotope ratios. Nature 405, 935–938.

Sarnthein, M., Tiedemann, R., 1990. Younger Dryas-style cooling events at glacial Terminations I–VI at ODP Site 658: Associated benthic $\delta^{13}C$ anomalies constrain meltwater hypothesis. Paleoceanography 5, 1041–1055.

Schiller, A., Mikolajewicz, U., Voss, R., 1997. The stability of the North Atlantic thermohaline circulation in a coupled ocean–atmosphere general circulation model. Clim. Dyn. 13, 325–347.

Schlitzer, R., 2000. Ocean Data View, http://www.awi-bremerhaven.de/GEO/ODV.

Schneider, R.R., Müller, P.J., Ruhland, G., 1995. Late Quaternary surface circulation in the east equatorial South Atlantic: Evidence from alkenone sea surface temperatures. Paleoceanography 10, 197–219.

Seidenkrantz, M.S., Kristensen, P., Knudsen, K.L., 1995. Marine evidence for climatic instability during the last interglacial in shelf records from northwest Europe. J. Quat. Sci. 10, 77–82.

Shipboard Scientific Party, 1999. Site 1089. In: Gersonde, R., Hodell, D.A., Blum, P. et al. (Eds.), Proc. ODP, Init. Rep. 177, pp. 1–36 (CD-ROM) (available from: ODP, Texas A&M University, College Station, TX).

Sieger, R., Gersonde, R., Zielinski, U., 1999. A new extended software package for quantitative paleoenvironmental reconstructions. EOS (Trans. Am. Geophys. Union), Electronic Suppl.

Sowers, T., Bender, M., 1995. Climate records covering the last deglaciation. Science 269, 210–214.

Steig, E.J., Brook, E.J., White, J.W.C., Sucher, C.M., Bender, M.L., Lehman, S.J., Morse, D.L., Waddington, E.D., Clow,

G.D., 1998. Synchronous climate changes in Antarctica and the North Atlantic. Science 282, 92–95.

Thompson, L.G., Davis, M.E., Mosley-Thompson, E., Sowers, T.A., Henderson, K.A., Zagorodnov, V.S., Lin, P.N., Mikhalenko, V.N., Campen, P.K., Bolzan, J.F., Cole-Dai, J., Francou, B., 1998. 25,000-year tropical climate history from Bolivian ice cores. Science 282, 1858–1864.

Thomson, D.J., 1982. Spectrum estimation and harmonic analysis. IEEE Proc. 70, 1055–1096.

Thouveny, N., de Beaulieu, J.L., Bonifay, E., Creer, K.M., Guiot, J., Icole, M., Johnsen, S., Jouzel, J., Reille, M., Williams, T., Williamson, D., 1994. Climate variations in Europe over the past 140 kyr deduced from rock magnetism. Nature 371, 503–506.

von Grafenstein, U., Erlenkeuser, H., Müller, J., Jouzel, J., Johnsen, S., 1998. The cold event 8200 years ago documented in oxygen isotope records of precipitation in Europe and Greenland. Clim. Dyn. 14, 73–81.

Welander, P., 1986. Thermohaline effects in the ocean circulation and related simple models. In: Willebrand, J., Anderson, D.T.L. (Eds.), Large-Scale Transport Processes in Ocean and Atmospheres. Reidel, Dordrecht, pp. 163–200.

White, W.B., Peterson, R.G., 1996. An Antarctic circumpolar wave in surface pressure, wind, temperature and sea-ice extent. Nature 380, 699–702.

Winograd, I.J., Szabo, B.J., Coplen, T.B., Riggs, A.C., 1988. A 250,000-year climatic record from Great Basin Vein Calcite: Implications for Milankovitch theory. Science 242, 1275–1280.

Woillard, G.M., 1978. Grande Pile peat bog: A continuous pollen record for the last 140,000 years. Quat. Res. 9, 1–21.

Yiou, P., Genthon, C., Ghil, M., Jouzel, J., Treut, H.L., Barnola, J.M., Lorius, C., Korotkevitch, Y.N., 1991. High-frequency paleovariability in climate and CO_2 levels from Vostok ice core records. J. Geophys. Res. 96, 20365–20378.

Yiou, P., Ghil, M., Jouzel, J., Paillard, D., Vautard, R., 1994. Nonlinear variability of the climatic system from singular and power spectra of Late Quaternary records. Clim. Dyn. 9, 371–389.

Zhao, M., Beveridge, N.A.S., Shackleton, N.J., Sarnthein, M., Eglinton, G., 1995. Molecular stratigraphy of cores off northwest Africa: Sea surface temperature history over the last 80 ka. Paleoceanography 10, 661–675.